ELSEVIER

Physics of the Earth and Planetary Interiors 106 (1998) 191–218

PHYSICS OF THE EARTH AND PLANETARY INTERIORS

Centroid-moment-tensor solutions for deep earthquakes predating the digital era: Discussion and inferences

Wei-Chuang Huang [1], Emile A. Okal *

Department of Geological Sciences, Northwestern University, Evanston, IL 60208, USA

Received 30 June 1997; revised 6 October 1997; accepted 8 October 1997

Abstract

We present a discussion of 139 new centroid-moment-tensor solutions for deep earthquakes covering the WWSSN (1962–1976) and earlier years, obtained by applying the standard Harvard inversion algorithm to data sets of seismograms digitized from analog records. Our solutions fill several gaps in seismicity reflecting undersampling by the Harvard catalogue. While most focal mechanisms previously published for WWSSN-era earthquakes are in good agreement with our inverted solutions, focal geometries for older events appear unreliable. We confirm that the region of most intense moment release is around 650 km, and that a minimum exists at 500 km. However, the local maximum around 450 km may be less marked than previously suggested. The Bonin–Marianas subduction zone exhibits a different pattern with an overall maximum of seismic activity at 420 km. All other subduction zones demonstrate the potential for seismicity at least at the 10^{27} dyn-cm level. Finally, while non-double-couple components are found systematically in our enhanced data set, they correlate neither with depth nor with earthquake size, suggesting that their presence does not necessarily relate to the exiguity of the space available for rupture at the tip of subduction zones.

Keywords: Centroid-moment-tensor solution; Seismicity; Deep earthquake; Subduction zone

1. Introduction and background

The purpose of this paper is to analyze and discuss the results of a systematic compilation of centroid-moment-tensor (CMT) solutions for deep earthquakes predating the development of digital seismic networks. The rationale of this project has been to extend the Harvard CMT catalogue (Dziewonski and Woodhouse, 1983 and subsequent quarterly updates) backwards in time in an effort to alleviate its only shortcoming, namely its relative youth. At present, the CMT catalogue covers only the past 20 years, thus undersampling the seismic cycle, as demonstrated by the fact that the largest earthquake in the catalogue (the 1977 Indonesian earthquake) remains 100 times smaller in moment than the 1960 Chilean event.

The quantification of older events usually involves various magnitude scales, plagued by both saturation and significant inconsistency between scales. This is especially true in the case of deep

* Corresponding author.

[1] Department of Physics, New Mexico State University, Las Cruces, NM 88003.

0031-9201/98/$19.00
PII S0031-9201(97)00111-8

earthquakes, which excite surface waves inefficiently, and for which the only available magnitudes are shorter period body-wave scales, known to saturate at even smaller source sizes than the standard surface-wave magnitude M_S (Geller, 1976).

On the other hand, CMT solutions can be obtained for deep earthquakes ($h \geq 300$ km) from extremely depleted data sets (consisting of as few as two components from a single station), following the exact same algorithm used routinely in the Harvard CMT project. This is explained by the abundant excitation of overtones by deep earthquakes, which bring to the seismic signal a variety in their kernels and hence a resolution which, in the case of shallower sources, would require either a large number of stations with good azimuthal repartition, or full coverage over a very broad band of frequencies. The theoretical justification of single-station inversions can be found in Buland and Gilbert (1976), and was tested (on a shallow earthquake, but using a broadband seismogram) by Ekström et al. (1986). More details about the procedure of applying the CMT algorithm to deep historical earthquakes, as well as detailed feasibility tests can be found in Huang et al. (1994) and Huang (1996).

In practice, we distinguish between the 'WWSSN era' (1962–1976), for which relatively abundant data with good sensitivity are available, and the 'historical' period (before 1962) when our sampling of the earthquake population reflects the irregular availability of seismograms. We obtained 104 CMT solutions for the WWSSN era and 35 for historical earthquakes. The WWSSN data set is believed to be complete above the moment threshold $M_0 \geq 2.5 \times 10^{25}$ dyn-cm, whereas the historical data set retains an ad hoc character and has no claim of completeness. The two data sets were published separately in the exact format of the quarterly Harvard reports (Huang et al., 1997, 1998).

In the next sections, we analyze some of the most interesting events in our data set, we compare our results to the mechanisms and moments occasionally published in the literature, and we discuss some inferences on the process of deep seismic release that can be drawn from our new solutions. We occasionally include in our discussion four earthquakes (Honshu, 1906; Perù, 1921; Fiji, 1932; and Spain, 1954) for which moment tensors were derived in independent studies, but which were kept out of our catalogue for the sake of preserving its homogeneity, since these solutions were obtained through a variety of methods, rather than through the application of the exact Harvard algorithm. These four solutions are listed in Table 4 of Huang et al. (1998).

2. Discussion of the most significant events

We select here for discussion a few cases which bring a new, or corrected, insight to various questions relating to the distribution of earthquakes in individual Wadati–Benioff Zones (WBZs). We are particularly attentive to the question of the robustness of spatial gaps apparent in the Harvard catalogue (and to whether or not they are artifacts of undersampling), to the lateral repartition of seismicity along WBZs (the plotting of selected historical earthquakes on maps such as the Plate Tectonic Map of the Circum-Pacific Region (American Association of Petroleum Geologists, 1987) would suggest that large earthquakes tend to occur at the edges of subduction zones), and to the documentation of 'outboard' earthquakes occurring in front of the WBZs in possibly detached elements of subducting lithosphere (see Lundgren and Giardini, 1994 for a review of modern events with such geometries). The following discussion is organized by region.

2.1. Korea to Kamchatka

Our CMT solutions for this region are shown on Fig. 1; we earmark as most significant the following earthquakes.

2.1.1. 25 May 1907; 52.5°N, 152.0°E, $h = 548$ km; $M_0 = 3.7 \times 10^{27}$ dyn-cm

This event is listed by Gutenberg and Richter (1954) and hence by the NEIC at 51.5°N, 147°E, and assigned a depth of 600 km. Should this location be confirmed, this would make it an outboard event located under the central Sea of Okhotsk, several hundred km in front of the WBZ. The data set of available arrival times is very poor, making it impossible to obtain a reliable relocation based on avail-

able bulletin listings of presumed P wave arrivals. Indeed, a special request to the ISC to reprocess the available list of arrivals resulted in a failure to obtain convergence of their algorithm to a definite solution [R.D. Adams, personal communication, 1995]. Rather, a systematic grid-search approach, consisting of trying many inversions for various constrained positions of the epicenter (Huang, 1996; Huang et al., 1998) resulted in moving the preferred location more than 300 km eastwards, to 52.5°N, 152°E, in the center of the WBZ and only slightly to the East of the large 1970 shock. The inverted focal mechanism is also is agreement with the latter's. The relocation vector is shown as the dashed line on Fig. 1.

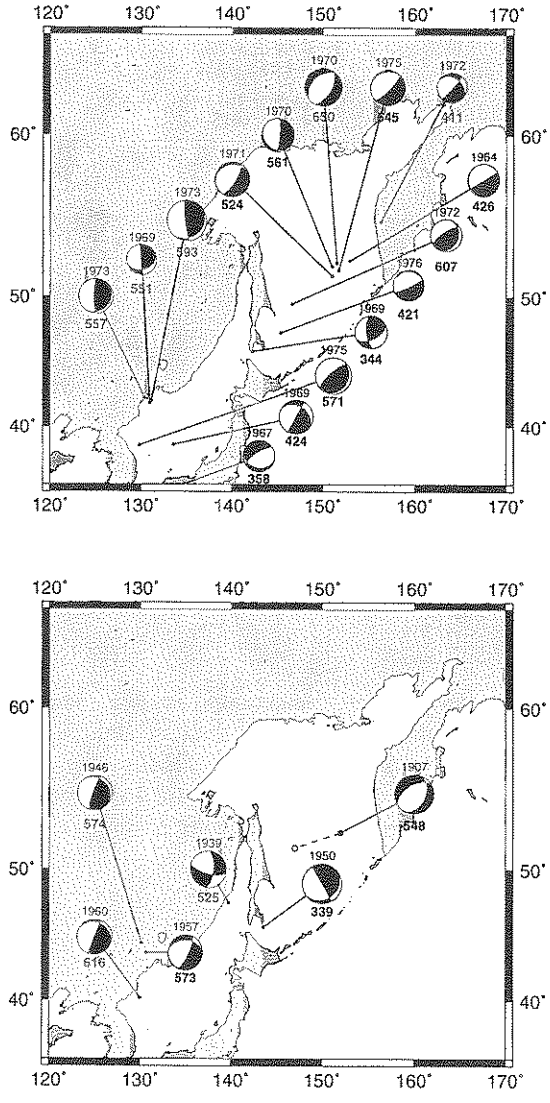

Fig. 1. Map of our new CMT solutions for the Korea-to-Kamchatka region. Top: WWSSN solutions. Bottom: Historical solutions. The year of each event is listed at the top of the beachball, and its depth (in **bold**) below it. The size of the beachball grows with the moment of the earthquake. The relocation vector of the 1907 earthquake is shown with dashes, from the NEIC location (open symbol) to the preferred epicenter (solid symbol).

2.1.2. 21 April 1939; 47.6°N, 139.75°E, h = 525 km; $M_0 = 4.3 \times 10^{26}$ dyn-cm

This earthquake took place under the Tatar Strait, between Sakhalin and the Maritime Province on mainland Asia. It is part of a finger of seismicity extending on the western side of the Sea of Okhotsk WBZ and identified by Okal et al. (1995) on the basis of 11 earthquakes (see Fig. 2). This argues for a contorted slab, rather than for the 1990 event being 'detached', as previously suggested. The deepest element of the finger is the Sakhalin deep earthquake of 12 May 1990. The focal mechanism of the 1939 event does not agree with that of its closest neighbor (the 1990 earthquake); however it must be noted that the recent CMT solutions in the finger are themselves not mutually compatible. The origin of the stress released in the Sakhalin finger is therefore unclear but the 1939 event confirms the significant level of moment release in this intriguing feature, as well as its apparent mechanical continuity.

2.1.3. 28 February 1950; 47.82°N, 143.55°E, h = 339 km; $M_0 = 3.9 \times 10^{27}$ dyn-cm

This event is the second largest historical (pre-1962) earthquake in our catalogue. It is also the largest event in its depth range (300–500 km) in that subduction system. It is interesting to note that it takes place in the general area of the Kuril–Hokkaido boundary, characterized by the occurrence of very large earthquakes outside the usual framework of shallow subduction-related interplate events (e.g., 04 October 1994, $h = 68$ km; $M_0 = 3 \times 10^{28}$ dyn-cm; 06 December 1978, $M_0 = 5.4 \times 10^{27}$ dyn-cm). The latter was found by Lundgren et al. (1988) to feature rupture extending as much as 90 km verti-

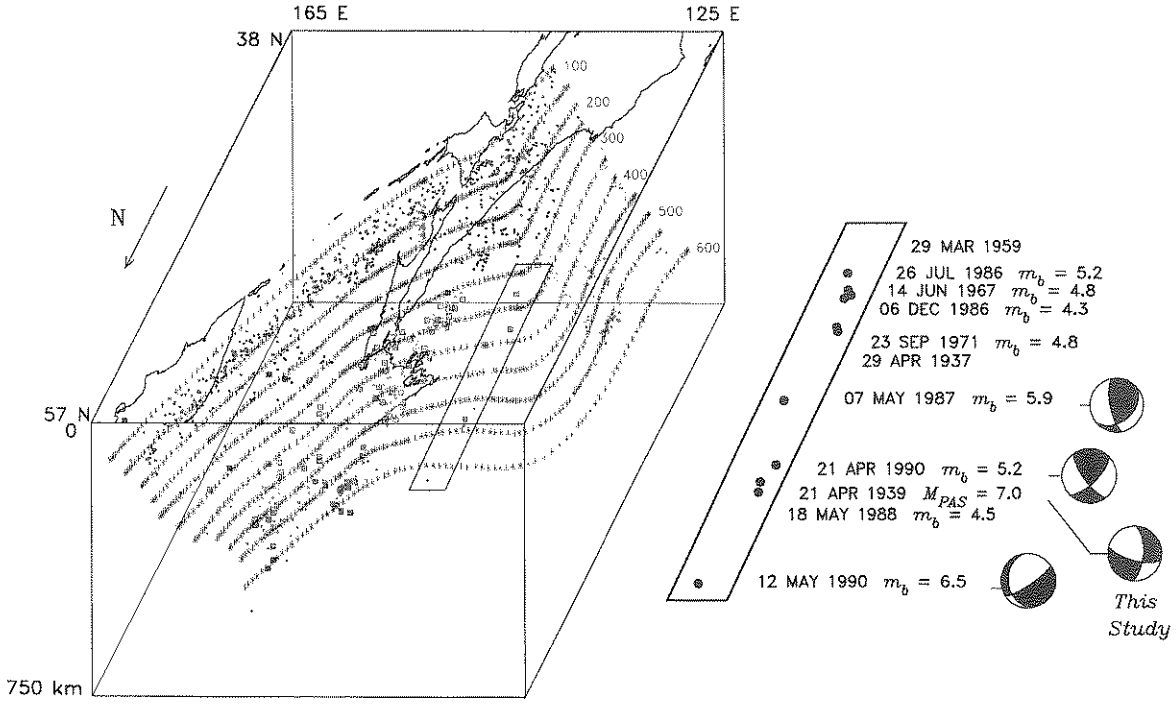

Fig. 2. Seismicity of the Kamchatka–Kuriles–Sea of Japan WBZ. This is a three-dimensional view looking South. The individual symbols correspond to hypocenters relocated by Okal et al. (1995); dots are modern events (1962–1993) and squares historical ones. The asterisks are lines of equal hypocentral depth best-fitting this dataset at 50-km intervals. The eleven earthquakes comprising the Sakhalin finger are outlined by the parallelogram and detailed at right with dates and available focal mechanism (Harvard CMT and this study). After Okal et al. (1995).

cally along one of its fault planes. It is worth noting that this fault plane is practically identical to that of the 1950 earthquake.

2.2. Izu–Bonin–Mariana Islands

2.2.1. 07 October 1968; 26.34°N, 140.24°E, $h = 490$ km; $M_0 = 1.14 \times 10^{27}$ dyn-cm

This is our largest solution in this region, and together with the events of 1951, 1955, 1956 to the North and the Harvard solution for 06 March 1984, it confirms that seismicity takes place regularly at the level of (5 to 11) $\times 10^{26}$ dyn-cm. As discussed more in detail below, it is remarkable that this maximum in seismic activity takes place in the Bonin Islands at shallower depths (440 to 490 km) than in other WBZs (except for the southernmost event, the 1955 shock, at 552 km). As well documented from more recent earthquakes, seismicity in the Marianas reaches significantly deeper than in the Northern (Bonin) section of that WBZ. Finally, no events larger than the 1968 earthquake are known in this subduction zone. The new data set is shown on Fig. 3a.

2.3. Philippines

No historical (pre-1962) events could be inverted. The only remarkable solution is the earthquake of 11 June 1972 under the Sea of Sulawesi ($h = 332$ km), which is the largest solution ($M_0 = 4.7 \times 10^{27}$ dyn-cm) in our whole data set above 500 km. This earthquake was recognized as especially large by Okal (1992) on the basis of mantle magnitude measurements. The geometry of subduction in this area

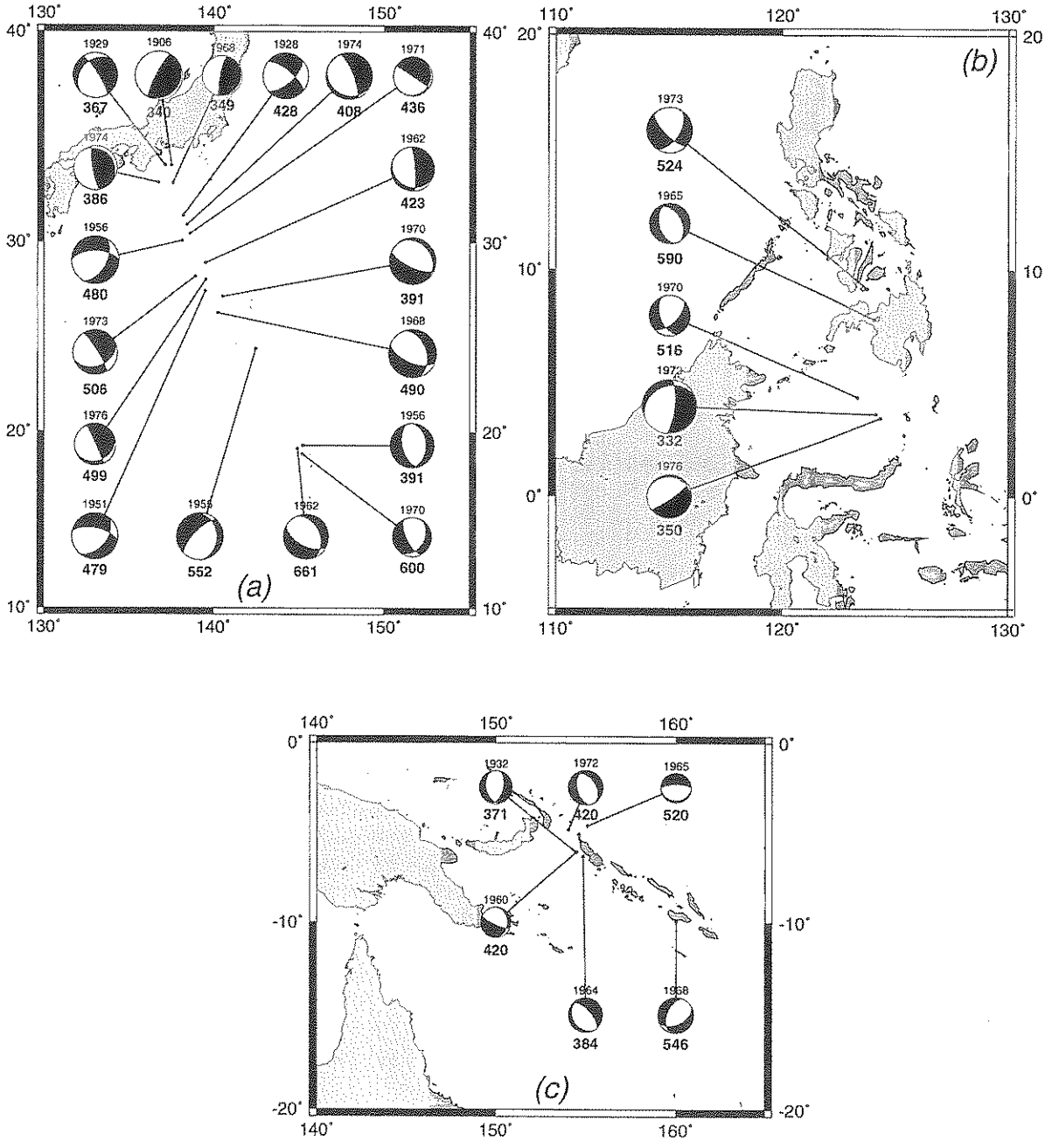

Fig. 3. Same as Fig. 1 for the Bonin–Marianas arc (a), the Philippines (b), and the Solomon Islands (c). WWSSN and historical solutions are plotted together on these maps.

is exceedingly complex but the pattern of seismicity would argue in favor of the event belonging to a westward-dipping slab. The new data set is shown on Fig. 3b.

2.4. Sunda Arc

Our CMT solutions are shown on Fig. 4. Among the most significant earthquakes are the following.

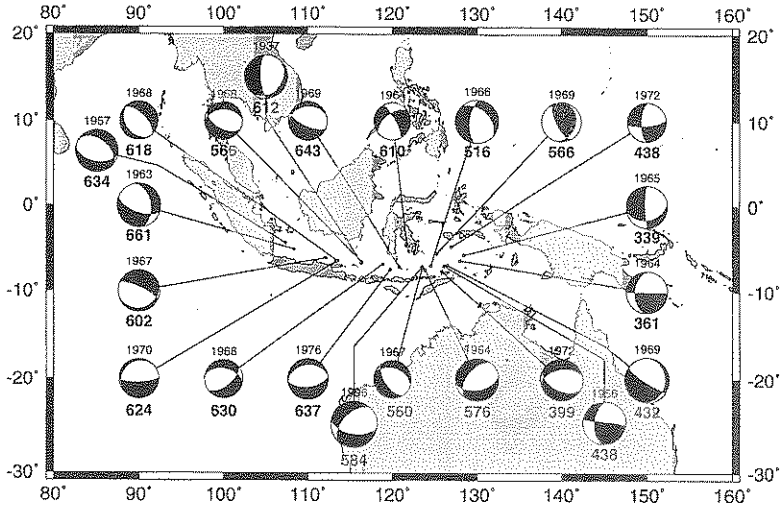

Fig. 4. Same as Fig. 1, for the Sunda Arc. Both WWSSN and historical solutions are plotted on this single map. Also shown is the 1996 Flores Sea deep earthquake.

2.4.1. 15 December 1963 (5.09°S, 108.33°E, $h = 661$ km; $M_0 = 4.5 \times 10^{26}$ dyn-cm) and 16 April 1957 (4.35°S, 107.30°E, $h = 636$ km; $M_0 = 2.6 \times 10^{26}$ dyn-cm)

These two events mark the western end of deep ($h \geq 300$ km) activity under the Sunda Arc. Kirby et al. (1996) have argued that the cessation of deep seismicity under the Java–Sumatra corner is related to the regular westward decrease in the age of the Indian Ocean floor subducting under the Sunda Arc. The large amplitude ($M_{PAS} = 7\frac{1}{2}$) assigned to the 1957 event by Gutenberg and Richter (1954) as reported in the NEIC data set) is one example raising the question of whether larger earthquakes in subduction zones are preferentially located near the lateral extremities of individual WBZs. While these two events are indeed large, the Pasadena magnitude of the 1957 event seems disproportionate.

2.4.2. 11 August 1937; 612 km; $M_0 = 5.0 \times 10^{26}$ dyn-cm

This event, about 1000 km further East, is generally comparable in size to the above two. However, this seismicity is dwarfed by the recent deep event under the Flores Sea (17 June 1996, $M_0 = 7.9 \times 10^{27}$ dyn-cm) which took place in the immediate vicinity of the bend in the subduction zone expressing the change in geometry from a perfectly vertical slab under the Bali Sea to a more sagging one under the Banda Sea. Based on the 1937, 1957, 1963 and 1996 events, the evidence is against the largest earthquakes occurring at the lateral boundaries of the Sunda WBZ.

2.5. Solomon Islands

The Harvard catalogue in this region is relatively poor in large earthquakes, with a maximum moment of 1.5×10^{26} dyn-cm (on 29 March 1980). We obtained six new solutions in this region, three of which of significantly larger size (13 August 1964, 6.19°S, 154.5°E, $h = 384$ km, $M_0 = 3.3 \times 10^{26}$ dyn-cm; 18 August 1968, 9.94°S, 160.00°E, $h = 546$ km, $M_0 = 9.8 \times 10^{26}$ dyn-cm; and 28 April 1972, 4.94°S, 154.09°E, $h = 420$ km, $M_0 = 7.8 \times 10^{26}$ dyn-cm) which clearly indicate undersampling by the Harvard catalogue.

2.6. Tonga–Fiji–Kermadec

We obtained no fewer than 45 new solutions in this region (35 WWSSN events and 10 historical ones). To prevent cluttering, these are shown in three different frames on Fig. 5. The overwhelming majority of these mechanisms follows the pattern of down-

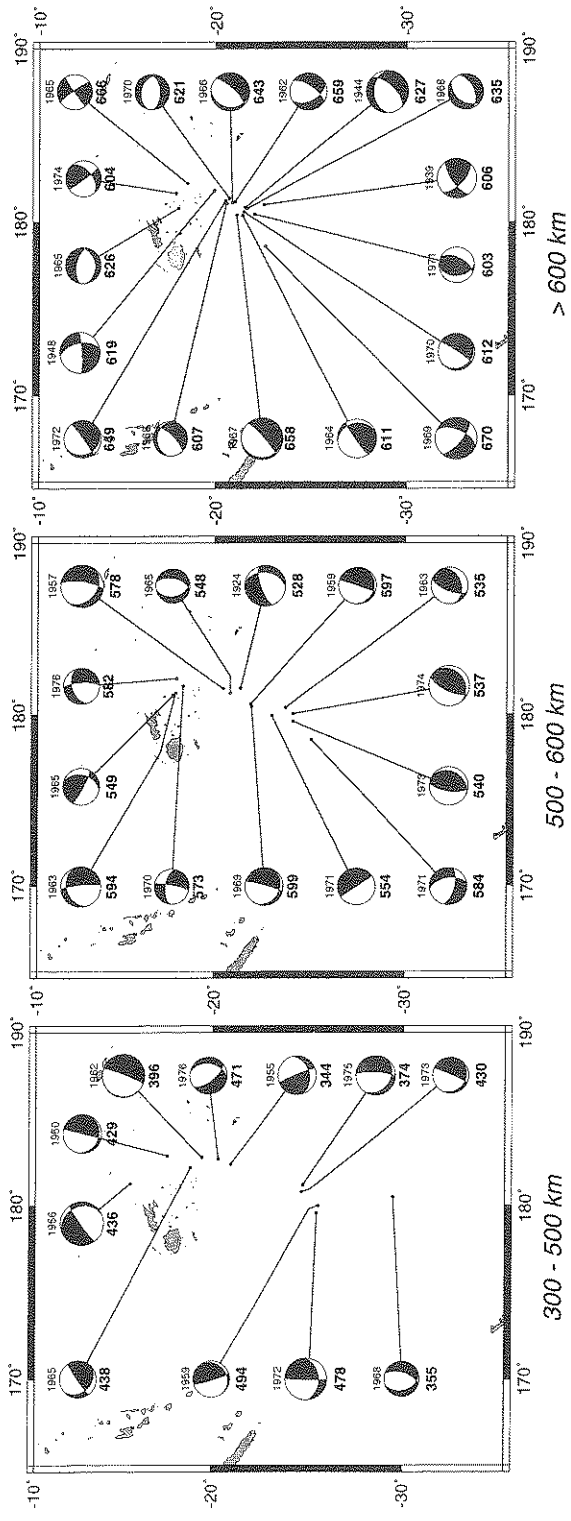

Fig. 5. Same as Fig. 1, for the Tonga–Fiji region. To avoid cluttering, the 45 inverted events are presented in three depth ranges.

dip compression first identified in the area by Isacks and Molnar (1971).

2.6.1. Above 500 km

The most significant event is the earthquake of 23 May 1956 (15.41°S, 178.73°W, $h = 436$ km, $M_0 = 2.7 \times 10^{27}$ dyn-cm). This shock, our northernmost solution in the region, took place on the bending side of the WBZ, in an area where no deep earthquake of comparable moment is known, the largest Harvard CMT solution (17 July 1978; $h = 322$ km) reaching only 7.1×10^{25} dyn-cm. The 1956 event indicates that the warping of the slab at the Samoa corner is accompanied by significant stress release even at substantial depths, a conclusion escaping the present Harvard CMT data set.

The remainder of the shallower seismicity is characterized by a few large events (21 May 1962, $M_0 = 9.3 \times 10^{26}$ dyn-cm); the gap in activity apparent in the Harvard data set between 20°S and 25°S is an artifact of sampling as demonstrated both by the 1955 solution and a recent event on 11 July 1992 ($M_0 = 7.8 \times 10^{26}$ dyn-cm).

2.6.2. Between 500 and 600 km

Our inverted events are concentrated in the Northern Fiji and Kermadec system with more modest moments ($M_0 \leq 4.4 \times 10^{26}$ dyn-cm). The absence in our catalogue of events comparable to the 1994 Fiji earthquake ($M_0 = 3 \times 10^{27}$ dyn-cm) is only an artifact of our failure to reliably invert the 1932 earthquake, for which an independent non-CMT solution is given by Okal (1997).

2.6.3. Below 600 km

Seismicity is characterized by a few large earthquakes taking place towards the bottom of the slab (09 October 1967, 21.12°S, 179.61°W, $h = 658$ km, $M_0 = 8.7 \times 10^{26}$ dyn-cm; 10 February 1969, 22.65°S, 178.69°E, $h = 670$ km, $M_0 = 8.3 \times 10^{26}$ dyn-cm). No seismicity of a comparable level is known in the area in the Harvard catalogue (a single event, on 26 May 1986 ($M_0 = 2.1 \times 10^{26}$ dyn-cm) is known above 10^{26} dyn-cm) and thus our study points out to significant undersampling in the latter. While not necessarily constituting an isolated earthquake in the sense of Lundgren and Giardini (1994), the 1969 earthquake resides at the extreme western arc of the Tonga WBZ; it is surrounded only by scarce seismicity as documented in post-1963 NEIC files.

2.7. Fiji Basin

2.7.1. 10 April 1965; (12.99°S, 170.54°E, $h = 631$ km; $M_0 = 3.3 \times 10^{25}$ dyn-cm) and 04 November 1968 (13.91°S, 171.87°E, $h = 594$ km; $M_0 = 6.9 \times 10^{25}$ dyn-cm)

West of the Tonga–Fiji system, we obtained solutions for these two events which belong to the Vityaz system. This group of earthquakes, undetected in early compilations of deep seismicity (Gutenberg and Richter, 1954), first recognized by Sykes (1964), and later analyzed by Barazangi and Dorman (1969), has been interpreted by Kirby and Okal (1996) as activity in a piece of slab originally part of the Vityaz subduction system to the North, but which became mechanically detached when subduction ceased at the Vityaz Trench about 8 Ma ago (Chase, 1971), and which now sits recumbent on the lower mantle. Our new mechanisms add to the extreme variety in focal mechanisms among deep Vityaz events (Fig. 6), which Kirby and Okal (1996) have interpreted as illustrating the absence of mechanically transmitted ambient stresses.

2.7.2. 01 October 1965; 20.27°S, 174.34°E, $h = 562$ km; $M_0 = 2.7 \times 10^{25}$ dyn-cm

Further to the Southeast, we inverted this small event, deep under the South Fiji Basin. While the earthquake is relatively isolated, two discrete fingers of deep seismicity are documented to the North and South, extending more or less horizontally from the Tonga–Fiji system and possibly related to lateral variations in the style of back-arc spreading under the Lau Basin (Kirby and Okal, 1996).

2.8. South America

Our South American data set is shown on Fig. 7. All solutions show down-dip compression, in agreement with the general character of the stress release in this province. We earmark the following earthquakes as most significant.

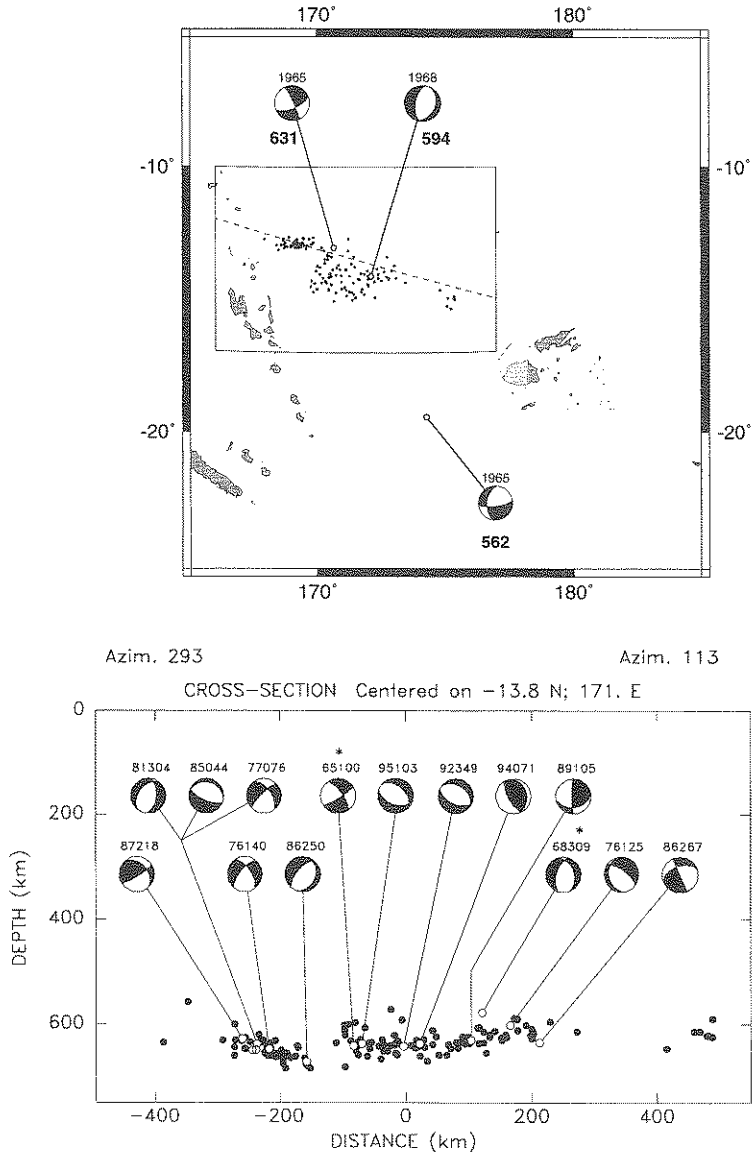

Fig. 6. Mechanisms in the Fiji Basin, between the Tonga and Vanuatu subduction system. Top: Map view. The light box identifies the region of the Vityaz cluster (Kirby and Okal, 1996). The individual dots are the events relocated by these authors. Bottom: Cross-section of the Vityaz cluster along the dashed line on the map. The mechanisms presented are from the Harvard catalogue, this study (asterisks) and other sources. Note the wide variety of geometries.

2.8.1. 28 April 1911; 9.5°S, 71.2°W, $h = 556$ km; $M_0 = 1.5 \times 10^{27}$ dyn-cm

As mentioned in Okal and Bina (1994) and Huang et al. (1994), this solution can converge only if the epicenter is relocated to the Peru–Brazil subduction segment. The NEIC listing at (0°N, 71.5°W; $h = 600$ km), which suggested some similarity with the 1970 Colombian event, is grossly in error. The relocation vector is shown as the dashed line on Fig. 7.

2.8.2. 17 January 1922; 3.8°S, 71.9°W, $h = 663$ km; $M_0 = 9.4 \times 10^{27}$ dyn-cm

This event, one of two studied in detail by Okal and Bina (1994), is located under the extreme North

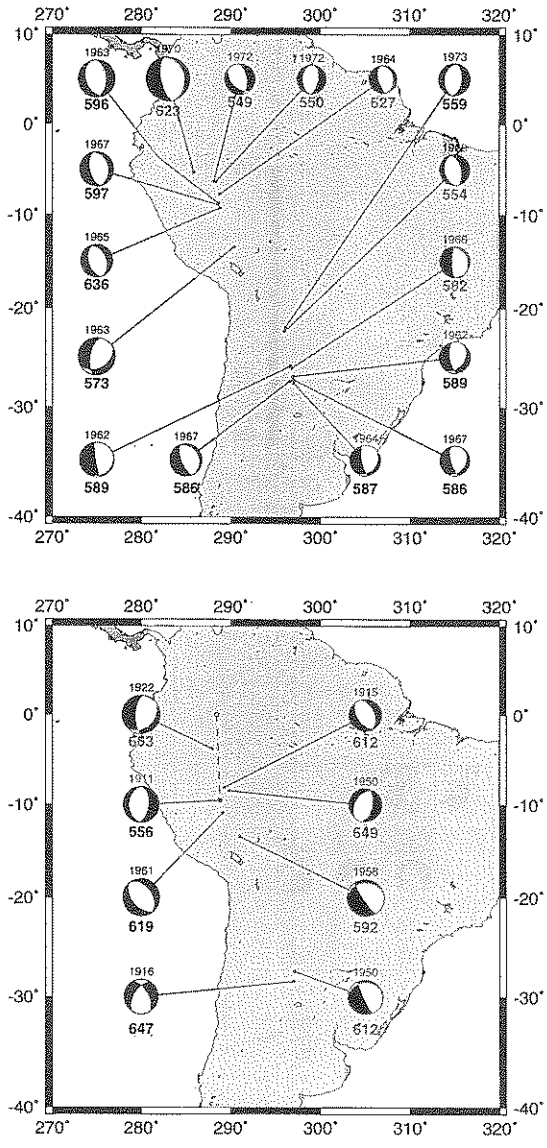

Fig. 7. Same as Fig. 1 for South America. The relocation vector of the 1911 event is shown as a dashed line.

of Peru, and these authors failed to identify any seismicity in its vicinity other than its precursor on 18 December 1921. Our inverted moment (9.4×10^{27} dyn-cm) is the largest one in our historical data set; it is however somewhat larger than Okal and Bina's solution (7×10^{27} dyn-cm) which may be a reflection of the different periods used in the two studies; at any rate, a discrepancy of only 25% in the moment of an event in the 1920s compares favorably with the scatter in estimates of large modern events such as the 1970 Colombian earthquake.

2.8.3. 26 July 1958; 13.5°S, 69.0°W, $h = 592$ km; $M_0 = 2.6 \times 10^{27}$ dyn-cm

This earthquake locates at the western limit of the East–West trending line of deep seismicity defined by Kirby et al. (1995) as the 'jog' linking and offsetting the Northern and Southern segments of the South American WBZ. It practically coincides with a shock in early 1994 and has a focal mechanism identical to that of the Bolivian aftershock of 08 August 1994, about 200 km to the East and at a comparable depth. It lies close to, but significantly below, the large event of 15 August 1963 studied by Gilbert and Dziewonski (1975), but it does not share its mechanism.

2.8.4. 21 June 1916; 28.5°S, 63.0°W, $h = 647$ km; $M_0 = 5.3 \times 10^{26}$ dyn-cm

This event, and its companion on 07 December 1912, are interesting in that they occur at the extreme Southern limit of the deepest activity in the South American WBZ. Both of them were assigned $M = 7\frac{1}{2}$ by Gutenberg and Richter (1954), which could suggest a trend towards increased event size at the extremity of the slab. However, our inverted moment remains much smaller than those of the 1958 and 1963 events in Peru, and is dwarfed by those of the large shocks of 1994 in Bolivia, 1922 in Northern Peru and 1970 in Colombia. Even though we were unable to reliably invert the 1912 event, examination of its record at Pulkovo, Russia, indicates that it cannot be significantly larger than the 1916 one. Furthermore, recent CMT solutions in the area indicate that seismicity above 10^{26} dyn-cm extends North to 25°S. Thus we do not detect any pattern of increased event size towards the southern edge of the Argentinian slab.

3. Comparison with results from previous studies

In this section, we compare the results in our catalogue with available solutions previously pub-

Table 1
Events with previously published focal mechanisms

Index	Date and time	Depth (km)	CMT solution				Published solution				Kagan angle (°)	Distances	
			M_0 (10^{26} dyn-cm)	ϕ (°)	δ (°)	λ (°)	ϕ (°)	δ (°)	λ (°)	References		P axes (°)	T axes (°)
WWSSN dataset													
1	7 Mar 1962, 1101	662	2.80	119	57	−112	148	49	−91	WH	24	20	16
2	21 May 1962, 2115	394	23.00	17	87	−85	15	84	−82	IM	5	3	6
3	10 Sep 1962, 1543	642	0.52	142	62	−142	147	43	−134	IM	20	18	13
4	29 Sep 1962, 1517	597	0.53	162	64	−99	164	63	−120	IM	23	14	17
5	7 Dec 1962, 1403	424	1.20	356	81	−73	180	78	32	WH	47	42	22
6	8 Dec 1962, 2127	590	6.10	173	84	−100	66	29	−10	S	20	18	6
7	15 Aug 1963, 1725	571	42.00	194	60	−115	188	53	−120	C	9	9	9
8	25 Aug 1963, 1218	599	3.80	355	84	−123	3	85	−120	ISO	8	7	6
9	8 Sep 1963, 1950	538	0.61	201	64	63	180	72	80	ISO	33	33	3
10	9 Nov 1963, 2115	595	32.00	1	50	−79	163	51	−95	F	13	10	12
11	15 Dec 1963, 1934	660	4.10	110	62	−125	125	56	−111	FM	15	15	5
12	18 Mar 1964, 0437	428	0.43	55	89	−82	141	36	172	A	29	23	16
13	21 Mar 1964, 0342	361	1.80	90	88	−48	86	83	−45	TB	7	3	7
14	13 Aug 1964, 0031	394	4.10	317	65	−95	134	36	−107	IM	20	20	11
15	18 Oct 1964, 1232	576	3.60	211	54	−125	83	50	−69	FM	19	12	14
16	25 Nov 1964, 0924	623	0.12	244	84	−35	208	70	20	O	72	43	66
17	28 Nov 1964, 1649	648	0.22	99	56	−129	154	52	−86	IM	45	38	26
18	9 Dec 1964, 1335	586	0.45	171	73	−104	171	78	−90	IM	15	11	11
19	28 Dec 1964, 1616	611	1.50	236	82	109	232	86	109	ISO	6	4	4
20	10 Apr 1965, 2232	552	0.57	121	80	57	113	87	46	ISO	14	0	15
20	10 Apr 1965, 2232	552	0.57	121	80	57	86	62	−175	O	63	62	48
22	22 May 1965, 1031	547	0.16	4	57	−80	108	60	−104	ISO	63	13	64
23	6 Jul 1965, 1836	511	0.28	269	72	−91	115	23	−62	ISO	10	9	4
25	20 Aug 1965, 0554	335	1.40	173	85	−127	81	31	6	FM	12	4	12
26	1 Oct 1965, 1322	565	0.23	82	74	−45	85	85	−54	ISO	15	7	16
27	3 Nov 1965, 0139	634	1.40	170	48	−89	169	50	−90	IM	2	2	2
28	18 Nov 1965, 2000	444	0.55	240	84	60	57	90	−90	ISO	31	25	18
29	9 Dec 1965, 1312	666	0.21	235	88	173	133	63	−39	ISO	48	50	2
30	25 Dec 1965, 0257	647	0.26	296	63	−81	70	47	−122	ISO	25	15	22
31	17 Mar 1966, 1550	648	1.10	46	72	−79	34	70	−86	ISO	12	10	6
32	22 Jun 1966, 2029	516	3.70	186	64	−61	178	63	−61	FM	8	3	8
33	20 Dec 1966, 1226	605	0.20	136	68	−105	163	72	−77	IM	32	31	8
34	17 Jan 1967, 0107	588	0.28	168	69	−110	161	68	−112	IM	7	6	6
35	15 Feb 1967, 1611	602	4.20	174	52	−88	168	49	−87	IM	8	2	8
36	24 Mar 1967, 0900	603	1.10	291	72	−60	109	24	−90	FM	30	24	19
37	13 Aug 1967, 2006	353	0.30	237	70	−107	88	20	−54	IM	10	2	10
39	9 Oct 1967, 1721	657	6.20	51	81	−85	54	86	−84	IM	6	6	5
40	9 Nov 1967, 0218	564	0.18	291	62	−56	54	45	−90	FM	47	32	35
41	20 Jan 1968, 2121	362	0.22	11	57	−66	4	57	−57	IM	14	6	13
43	28 Feb 1968, 1208	341	0.18	191	82	88	180	86	96	M	15	16	4
46	18 Aug 1968, 1838	545	9.40	201	51	−120	63	58	−51	R	13	13	9
49	7 Oct 1968, 1920	493	12.00	113	59	−120	119	63	−134	M	19	12	15
51	4 Nov 1968, 0907	607	0.68	190	58	−96	340	38	−120	IM	25	21	14
52	24 Jan 1969, 0233	602	1.00	19	84	−70	24	87	−68	WM	7	5	3
53	10 Feb 1969, 2258	667	7.10	142	62	−141	102	85	−117	D	57	9	56
55	31 Mar 1969, 1925	418	0.97	31	88	−130	37	84	−158	M	30	15	25
59	18 Dec 1969, 1332	346	0.46	174	68	36	157	65	30	SM	16	15	14
60	28 Jan 1970, 2306	618	0.24	76	58	−107	8	59	−62	D	82	12	83
65	31 Jul 1970, 1708	651	140.0	169	65	−90	148	58	−99	M	20	15	15

Table 1 (continued)

Index	Date and time	Depth (km)	CMT solution				Published solution				Kagan angle (°)	Distances P axes (°)	Distances T axes (°)
			M_0 (10^{26} dyn-cm)	ϕ (°)	δ (°)	λ (°)	ϕ (°)	δ (°)	λ (°)	References			
68	30 Aug 1970, 1746	645	12.00	37	53	−100	40	50	−90	SM	9	8	5
69	5 Sep 1970, 0752	561	0.78	22	81	−106	30	62	−68	SM	41	36	28
70	29 Jan 1971, 2158	524	2.50	28	74	−106	40	77	−119	SM	20	7	18
74	20 Nov 1971, 0728	556	0.69	322	90	−95	317	11	68	D	20	18	15
77	26 Jan 1972, 2300	665	0.82	52	88	−69	69	79	−90	D	31	12	29
78	30 Mar 1972, 0534	479	9.60	183	85	53	179	82	55	D	6	6	5
79	4 Apr 1972, 2243	398	1.90	261	50	−115	255	49	−118	FK	5	4	4
81	27 May 1972, 0406	465	0.13	38	89	−127	25	80	−100	SM	32	19	29
82	11 Jun 1972, 1641	336	38.00	6	74	−112	25	66	−90	FK	25	25	5
83	21 Aug 1972, 0623	624	0.29	237	63	111	18	15	44	SM	22	23	14
99	23 Jan 1976, 0545	637	1.10	68	56	−84	50	50	−90	FK	16	8	15
Historical dataset													
208	2 Jun 1929, 2138	367	2.50	327	80	−124	8	13	90	IM	58	58	33
210	11 Aug 1937, 0055	612	5.00	177	70	−107	67	39	−91	WH	67	31	58
211	21 Apr 1939, 0428	525	4.30	105	69	−152	108	32	−155	WH	37	25	32
214	11 Jan 1946, 0132	574	2.10	200	82	106	69	40	153	A	53	24	48
216	28 Feb 1950, 1020	339	39.00	150	89	68	286	74	−142	A	82	79	31
218	14 Aug 1950, 2250	612	5.60	155	82	−72	120	24	62	AR	42	38	35
219	22 Sep 1950, 2353	429	1.70	14	89	−74	319	85	17	R	102	58	82
220	11 Jul 1951, 1821	479	5.50	281	62	−49	85	29	−149	R	55	14	54
221	30 May 1955, 1231	552	7.00	224	70	−69	6	54	−148	I	34	33	21
223	1 Feb 1956, 1341	391	1.60	165	53	−100	116	69	−122	WH	45	30	34
224	18 Feb 1956, 0734	480	9.80	270	59	−47	28	63	−156	R	20	19	7
225	23 May 1956, 2048	436	27.00	234	84	−68	100	65	87	WH	55	34	47
227	3 Jan 1957, 1248	573	2.50	25	74	−121	69	33	161	A	76	33	71
228	16 Apr 1957, 0404	636	2.60	100	48	−109	148	59	306	OK	48	45	12
229	28 Sep 1957, 1420	578	16.00	8	73	−65	55	68	−88	WH	59	15	59
230	26 Jul 1958, 1737	592	26.00	145	80	−70	75	63	−96	WH	68	46	47
234	8 Oct 1960, 0552	616	2.10	202	89	108	344	31	44	AR	24	22	23
235	19 Aug 1961, 0509	620	34.00	140	49	−92	91	49	−15	WH	86	50	82

References: A: Averyanova (1973); AR: Ritsema (1965); C: Chandra (1970); D: Denham (1977); F: Fitch (1972); FK: Fukao and Kikuchi (1987); FM: Fitch and Molnar (1970); I: Ichikawa (1961); IM: Isacks and Molnar (1971); ISO: Isacks et al. (1969); M: Mikumo (1971); O: Oike (1971); OK: Okal and Kirby (1993); R: Ripper (1974); S: Stauder (1973); SM Stauder and Mualchin (1976); TB: Teng and Ben-Menahem (1965); WH: Wickens and Hodgson (1967); WM: Wyss and Molnar (1972).

lished in the literature. This effort follows in the footsteps of Giardini (1984) who, early in the life of the Harvard CMT project, compared inverted moment-tensor solutions for deep earthquakes with published first-motion mechanisms, which he found in generally good agreement.

Many of the larger earthquakes in our catalogue were the subject of individual studies in the late 1960s and early 1970s. These were mostly based on the then newly available WWSSN records, and their primary goal was the recovery of the orientation of the events' focal mechanisms; as such, the amplitude information, i.e., the value of the scalar moment, was most often not sought.

3.1. Focal mechanisms

A literature search resulted in the compilation of focal mechanisms for 78 among our 139 earthquakes (60 during the WWSSN years, and 18 older events). These solutions are listed in Table 1, along with the results of our inversions. The events are indexed

using the same numbers as in Table 1 of Huang et al. (1997) and Huang et al. (1998). Most of the published solutions are from the early works of Isacks et al. (1969) and Isacks and Molnar (1971), which were based mostly on WWSSN records; for the older events, focal solutions are mainly from Wickens and Hodgson (1967). In addition, a number of solutions were found in Denham (1977), itself a compilation of many different sources, but unfortunately limited to the Western Pacific. It is remarkable that more solutions are found in the early years of the WWSSN than in later ones. This undoubtedly reflects the waning of interest on the part of seismologists when the general pattern of the geometry of stress release was understood in the early 1970s.

The comparison of focal geometries can be quantified through the angular distance Δ between the inverted and previously published directions of, respectively, compressional (P) and tensional (T) axes (in all cases $0 < \Delta < 90°$). These axes are usually taken as representative of the state of stress of subducting slabs and have been of primary importance in the analysis of the driving forces of convection and of the rheology of the subducting lithosphere (Richter, 1979; Vassiliou, 1984). In Figs. 8 and 9, we present the angular distances Δ_P and Δ_T,

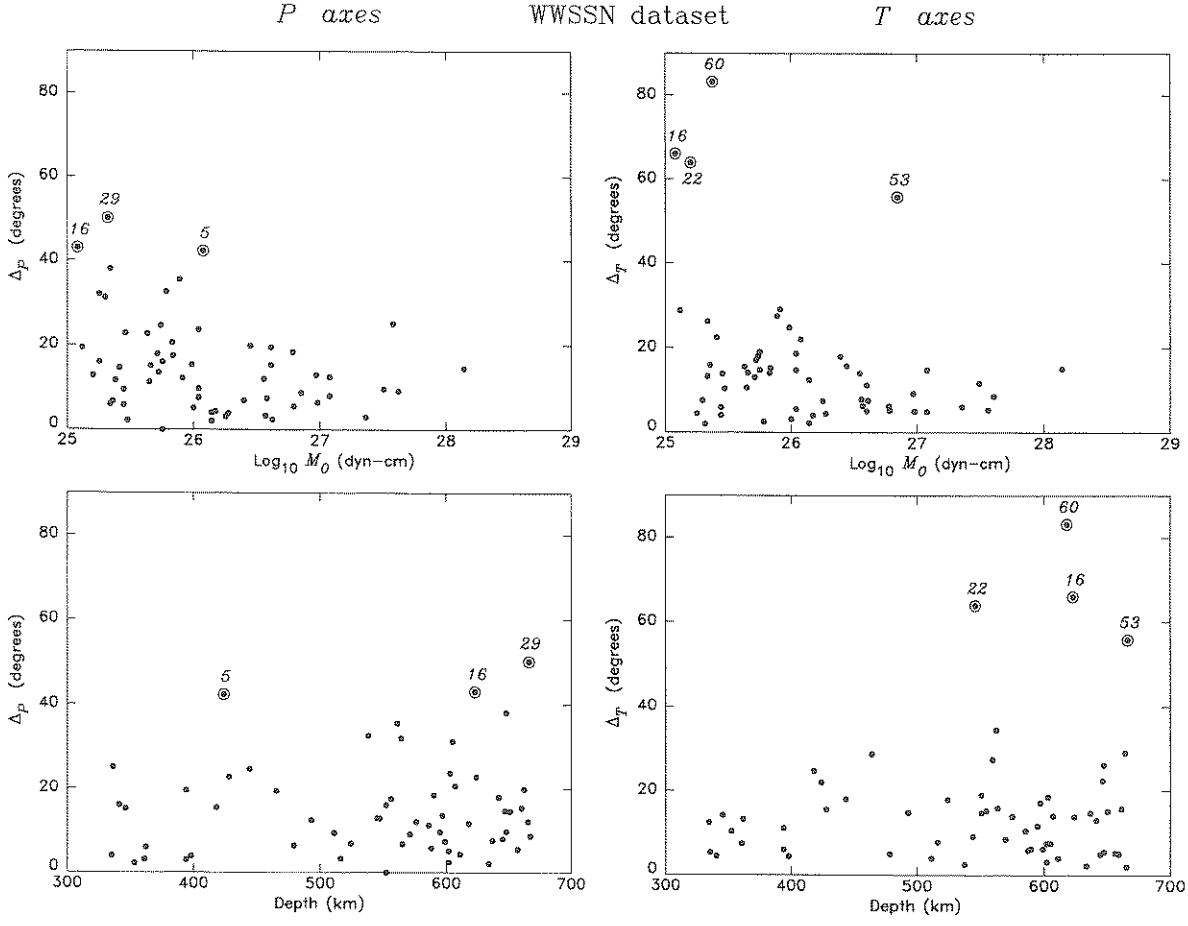

Fig. 8. Angular distance between inverted and previously published directions of compressional (Left) and tensional (Right) axes for the WWSSN dataset, plotted as a function of seismic moment (Top) and depth (Bottom). Events for which a significant discrepancy occurs are outlined and discussed in the text.

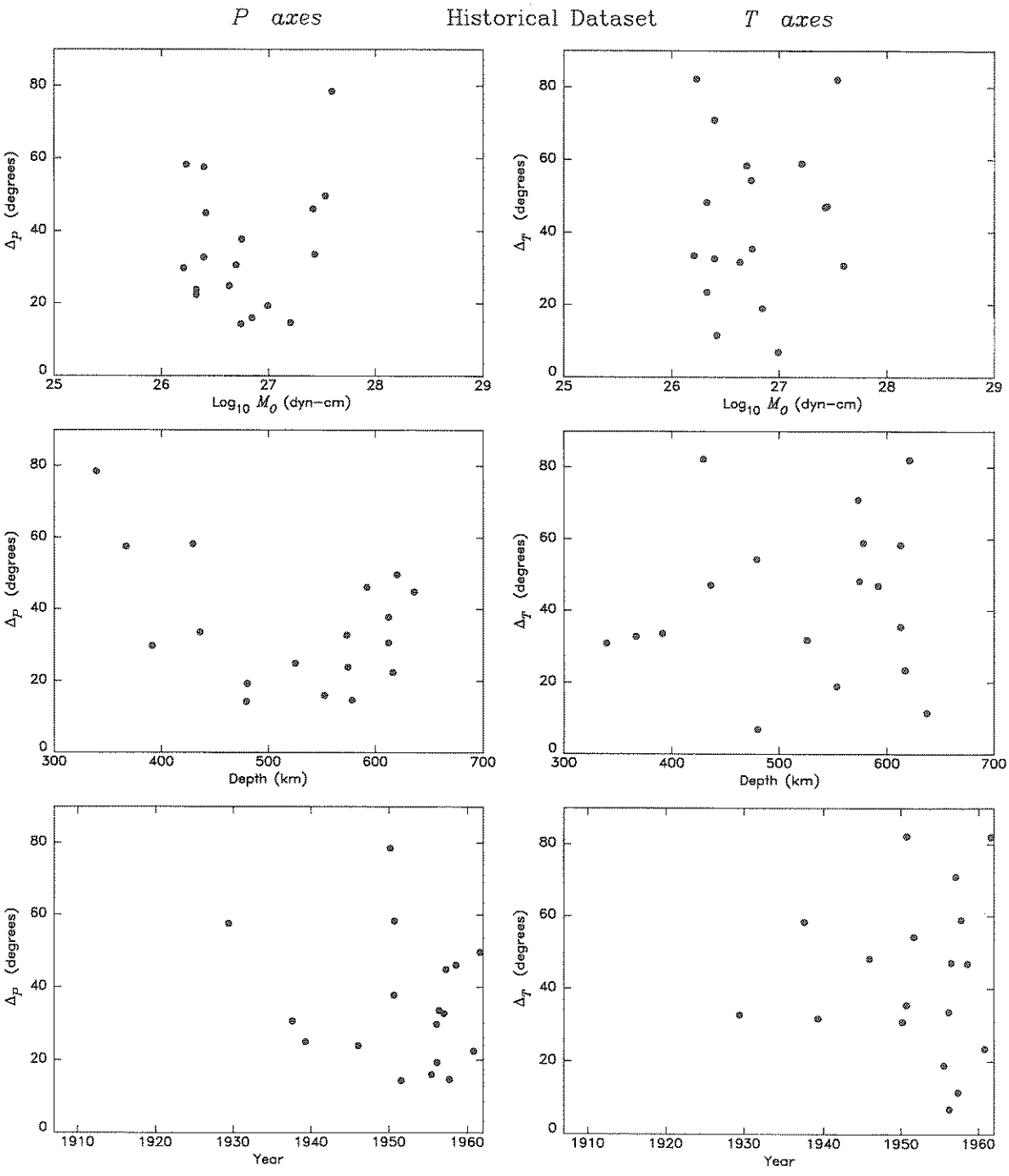

Fig. 9. Same as Fig. 8 for the historical dataset. The bottom frames examine a possible dependence on the age of the events. Note large scatter throughout the dataset.

as a function of inverted moment, depth and, for the older earthquakes, year. Following Kagan (1991), another more formal approach consists of computing the angle of the solid rotation necessary to reconcile the two mechanisms. For each of the 78 earthquakes, Table 1 lists (in its third-to-last column) the smallest among the four possible such angles.

With a few exceptions (detailed below), solutions published from WWSSN data are in generally good agreement with our moment-tensor solutions, the angle between the respective stress directions being typically less than 20°. This is in clear contrast with the older, historical data set, for which the agreement is at best poor, and at worst inexistent (Fig. 9).

For the WWSSN events, we detect a general increase in the quality of the published solutions with earthquake size, but a deterioration with increasing depth. When the angular distances between P and T axes are small, the Kagan angle is comparable to the larger of the two. For P axes, only three events (5, 16 and 29) exhibit differences of orientation greater than 40°. For T axes, four events (16, 22, 53 and 60) do. The case of Events 22 and 60 is reasonably well explained when comparing the beachballs on Fig. 10. A probable paucity of close-by stations would have led the early investigators to poorly constrained focal planes while correctly asserting the down-dip compressional nature of the events. In the case of Event 5, the published and CMT solutions have one nearly common fault plane which must have been well constrained in the first-motion solution, while the second plane has a much shallower dip in the inverted solution. In the case of the small strike-slip events 16 and 29, the exact position of the focal planes would be controlled by stations at core-grazing distances whose first motions may have been of questionable polarities, given the small magnitudes involved.

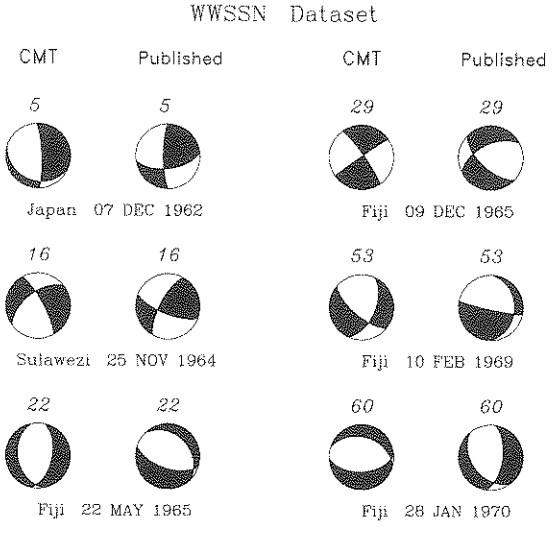

Fig. 10. Comparison of inverted mechanisms with previously published solutions, for those events exhibiting the largest differences in mechanisms.

Regarding the historical data set, Fig. 9 shows that the angles between directions of inverted and published principal stresses are scattered between 0 and 90°, with no apparent correlation with depth, earthquake size, or even, as one might have expected, with the age of the event. Furthermore, it is interesting to note that the older published mechanisms are often incompatible with the trends of stress release in the relevant WBZs, as documented by the Harvard CMT catalogue. In particular, many show deep mechanisms with tensional rather compressional axes close to the down-dip direction, whereas our CMT solutions are usually consistent with the orientation of modern earthquakes at comparable locations. Similarly, the Kagan rotation angles are very large for the historical data set, in general 45° or greater. A conclusion of this study is therefore that the data set of previously published mechanisms for historical (pre-1962) deep earthquakes is unsupported by our inversions and appears unreliable. This is especially true of the geometries listed in Wickens and Hodgson (1967): most of them were obtained in the early 1960s, before the representation of the earthquake source as a double-couple was firmly established. The catalogue of Denham (1977), on the other hand, fares somewhat better in comparison to our solutions.

3.2. Seismic moments

A number of deep earthquake moments were obtained in the late 1960s and 1970s, using several methods such as the modeling of the spectral amplitude of surface waves, the modeling of body waveforms and the interpretation of the spectrum of body waves in terms of a corner frequency representative of the dimensions of the source, in turn related to the

Table 2
Events with previously published seismic moments

Index	Date	CMT moment	Published moment		
		M_0 (dyn-cm)	M_0 (dyn-cm)	Technique	References
WWSSN dataset					
4	29 Sep 1962	5.3×10^{25}	1.5×10^{26}	P waves	W
6	8 Dec 1962	6.6×10^{26}	3.8×10^{26}	P waves	W
6	8 Dec 1962	6.6×10^{26}	1.2×10^{27}	Surface waves	W
7	15 Aug 1963	3.9×10^{27}	1.4×10^{28}	Surface waves	W
7	15 Aug 1963	3.9×10^{27}	4.2×10^{27}	Normal modes	GD
7	15 Aug 1963	3.9×10^{27}	6.9×10^{27}	Surface waves	FF
8	25 Aug 1963	4.4×10^{26}	8.8×10^{26}	P waves	BJ
10	9 Nov 1963	3.5×10^{27}	3.1×10^{27}	Surface waves	W
10	9 Nov 1963	3.5×10^{27}	7.4×10^{26}	P waves	W
10	9 Nov 1963	3.5×10^{27}	8.3×10^{26}	Surface waves	FF
13	21 Mar 1964	1.8×10^{26}	3.0×10^{26}	Body waves	TB
17	28 Nov 1964	5.3×10^{24}	9.7×10^{24}	P waves	BJ
18	9 Dec 1964	4.0×10^{25}	8.7×10^{25}	P waves	W
18	9 Dec 1964	4.0×10^{25}	3.0×10^{25}	Surface waves	W
20	10 Apr 1965	3.3×10^{25}	3.5×10^{25}	Body waves	WM
25	20 Aug 1965	1.5×10^{26}	1.6×10^{26}	Surface waves	W
27	3 Nov 1965	1.4×10^{26}	1.2×10^{26}	P waves	W
28	18 Nov 1965	6.0×10^{25}	3.4×10^{25}	Body waves	WM
31	17 Mar 1966	1.2×10^{26}	1.2×10^{26}	Body waves	WM
32	22 Jun 1966	3.6×10^{26}	7.0×10^{25}	Body waves	O
33	20 Dec 1966	3.4×10^{25}	3.8×10^{25}	P waves	W
38	9 Sep 1967	1.5×10^{26}	8.7×10^{25}	P waves	W
39	9 Oct 1967	8.7×10^{26}	5.7×10^{26}	P waves	S
41	20 Feb 1968	2.0×10^{25}	2.0×10^{25}	Body waves	WM
43	28 Feb 1968	3.0×10^{25}	3.6×10^{25}	Body waves	M
49	7 Oct 1968	1.1×10^{27}	1.6×10^{27}	Body waves	M
55	31 Mar 1969	1.2×10^{26}	1.7×10^{26}	Body waves	M
59	18 Dec 1969	4.2×10^{25}	1.0×10^{26}	Body waves	M
63	27 May 1970	5.9×10^{26}	8.0×10^{26}	Body waves	M
65	31 Jul 1970	1.4×10^{28}	2.1×10^{28}	Surface waves	FF
65	31 Jul 1970	1.4×10^{28}	1.8×10^{28}	Normal modes	GD
68	30 Aug 1970	1.1×10^{27}	1.1×10^{27}	P waves	S
69	5 Sep 1970	6.5×10^{25}	6.4×10^{25}	P waves	S
70	29 Jan 1971	2.5×10^{26}	2.8×10^{26}	P waves	S
78	30 Mar 1972	9.3×10^{26}	3.7×10^{26}	P waves	S
82	11 Jun 1972	4.7×10^{27}	3.8×10^{27}	Mantle magnitude	EO
87	10 Sep 1973	1.2×10^{26}	1.5×10^{26}	P waves	K
89	29 Sep 1973	5.0×10^{27}	6.4×10^{27}	Surface waves	FF
92	22 Feb 1975	2.3×10^{26}	2.1×10^{26}	P waves	S
Historical dataset					
216	28 Feb 1950	3.9×10^{27}	3.1×10^{27}	Mantle magnitude	EO
225	23 May 1956	2.7×10^{27}	9.8×10^{26}	Mantle magnitude	EO
230	26 Jul 1958	2.6×10^{27}	2.8×10^{27}	Surface waves	W

References: BJ: Berckhemer and Jacob (1968); EO: Okal (1992); FF: Furumoto and Fukao (1976); GD: Gilbert and Dziewonski (1975); K: Koyama (1976); M: Mikumo (1972); O: Oike (1969); S: Sasatani (1980); TB: Teng and Ben-Menahem (1965); W: Wyss (1970); WM: Wyss and Molnar (1972).

moment. It is interesting to compare these early measurements with the results of our systematic CMT inversions. A literature search yielded the 42 moment values listed in Table 2 for 35 of the earthquakes investigated in the present study. A large proportion were taken from the studies of Wyss (1970) and Wyss and Molnar (1972) for deep events in, respectively, the South American and Tonga–Kermadec subduction zones. This includes only one event predating the WWSSN, namely the Peru–Bolivia deep shock of 26 July 1958.

In three occasions for which no moment could be found in the literature, we list estimates from computations of the mantle magnitude M_m by Okal (1992); for two of them, the agreement is excellent. In the case of the earthquake of 23 May 1956 in Fiji, Okal's estimate (0.98×10^{27} dyn-cm) is significantly lower than ours (2.7×10^{27} dyn-cm); this is however easily explained by noticing that the station used in Okal's study (PAS) falls in a node of radiation of Rayleigh waves for our inverted mechanism. At any rate, M_m is expected to provide only an order of magnitude of the seismic moment.

Fig. 11 compares our CMT-derived moments with previously published values. When several values were published for a single event, they are connected by a vertical line. The quality of the previously available moments can be assessed through the logarithmic residual

$$r = \log_{10} \frac{M_0^{PP}}{M_0^{CMT}} \quad (1)$$

where M_0^{PP} and M_0^{CMT} are, respectively, the values previously published and inverted in the present study. The absolute average value, $|\langle r \rangle|$ is less than 0.01, which means that the older estimates are not systematically biased towards values higher or lower than CMT-inverted moments. However, both the standard deviation $\sigma_r = 0.28$ of the r population, or the average of the absolute values, $\langle |r| \rangle = 0.20$ (amounting to an average multiplicative or divisive factor of 1.6), indicate that the older estimates are significantly scattered away from the modern value of the seismic moments. Interestingly and somewhat unexpectedly, these numbers are not significantly affected when the population is separated into original measurements obtained by body wave techniques ($\langle r \rangle = -0.00$, $\langle |r| \rangle = 0.20$, $\sigma_r = 0.28$) and by longer period methods (surface waves, normal modes, mantle magnitude; $\langle r \rangle = 0.01$, $\langle |r| \rangle = 0.20$, $\sigma_r = 0.27$).

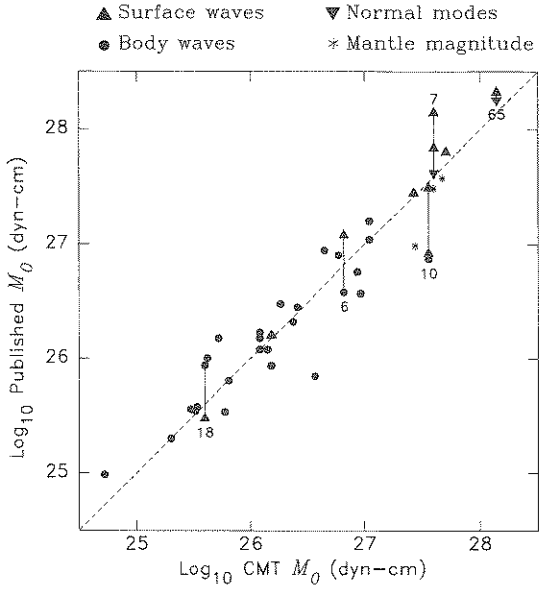

Fig. 11. Comparison of inverted and previously published seismic moments for events in the WWSSN dataset. The various symbols refer to different methods used to compute M_0 in earlier studies. When several values were published, they are linked by a vertical line, and the event index refers to Table 2.

As evidenced by the splitting of the population in its halves of lower and higher moments, a slight trend exists, however, for the older values to both overestimate smaller earthquakes and underestimate the larger ones (both by about 10%), and also to exhibit a generally greater scatter for large events with respect to CMT-derived values. The larger moments were estimated by the older techniques with an accuracy which is no better, on the average, than a multiplicative or divisive factor of 1.7.

Finally, the scatter can be considerable among previously published values for the same event, when several moments are available. In the case of the Peruvian earthquake of 09 November 1963 (Event 10), for example, a factor of 4.5 separates the extreme estimates by Wyss (1970) and by Furumoto and Fukao (1976), even though both studies were

based on surface waves. The present study is in excellent agreement with the latter. These few examples clearly illustrate the difficulties inherent in the use of an inhomogeneous data set such as that of previously published moments and reaffirm the superior value of the homogeneous population of CMT-derived moments obtained in the present study.

4. Depth distribution of seismicity

In this section, we address the question of the repartition of seismic release with depth inside slabs. This subject is important since any attempt to understand the origin and mechanism of stress release in deep earthquakes should in particular explain its variation with depth, both on a global scale and possibly in individual subduction zones.

4.1. The largest events

Table 3 lists the largest measured seismic moments in the two depth ranges 300–500 km and ≥ 500 km. In both instances, the number of earthquakes chosen (10 and 13, respectively) corresponds to a natural break in the populations. For the sake of completeness, we have included non-CMT solutions in this data set but flagged them with a dagger (†) to indicate their special character. The value of the present study is immediately realized by noticing that seven out of 10 events in Table 3a and 11 out of 13 in Table 3b predate the digital CMT database. Furthermore, when this study was started in 1993, the largest available CMT solution below 500 km was for the event of 05 March 1984 under Mindanao, which at 9.3×10^{26} dyn-cm, would not make the top 15 group in our enhanced data set.

Table 3

(a) Moderately deep earthquakes ($300 \leq h \leq 500$ km) with the 10 largest moments for 1906–1994

Rank	Index	Date	Area	Depth (km)	Moment (dyn-cm)
1	82	11 Jun 1972	Celebes sea	332	4.7×10^{27}
2	216	28 Feb 1950	Sea of Okhotsk	339	3.9×10^{27}
3	225	23 May 1956	Fiji Islands	436	2.7×10^{27}
4	2	21 May 1962	Fiji Islands	396	2.0×10^{27}
5		22 Jun 1982	Banda Sea	473	1.8×10^{27}
6	†	21 Jan 1906	Honshu	340	1.5×10^{27}
7		06 Mar 1984	Honshu–Bonin	446	1.4×10^{27}
8	49	07 Oct 1968	Bonin Islands	490	1.1×10^{27}
9		21 Jul 1994	Sea of Japan	489	1.1×10^{27}
10	224	18 Feb 1956	Honshu–Bonin	480	9.8×10^{26}

(b) Very deep earthquakes ($h \geq 500$ km) with the 13 largest moments for 1907–1996

Rank	Index	Date	Area	Depth (km)	Moment (dyn-cm)	Environment
1		09 Jun 1994	North Bolivia	647	2.6×10^{28}	Bend
2	65	31 Jul 1970	Colombia	623	1.4×10^{28}	Isolated
3	205	17 Jan 1922	North Peru	664	9.4×10^{27}	Isolated
4		17 Jun 1996	Flores Sea	589	7.9×10^{27}	Bend
5	†	29 Mar 1954	Spain	630	7.0×10^{27}	Isolated
6	89	29 Sep 1973	North Korea	593	5.0×10^{27}	Bend/edge
7	†	26 May 1932	Fiji	560	4.0×10^{27}	Bend
8	7	15 Aug 1963	Peru–Bolivia	573	3.9×10^{27}	Bend
9	201	25 May 1907	Sea of Okhotsk	548	3.7×10^{27}	
10	10	09 Nov 1963	Peru–Bolivia	573	3.5×10^{27}	
11	235	19 Aug 1961	Peru–Bolivia	620	3.4×10^{27}	
12		09 Mar 1994	Fiji	563	2.7×10^{27}	
13	230	26 Jul 1958	Peru–Bolivia	592	2.6×10^{27}	Bend

† = Non-CMT solutions. See Section 4.1.

Table 4
Largest known deep events ($h \geq 500$ km) for each subduction zone

Region	Date	Index	Depth (km)	Moment (dyn-cm)
South America	09 Jun 1994		647	2.6×10^{28}
Indonesia	17 Jun 1996		589	7.9×10^{27}
Spain	29 Mar 1954	†	630	7.0×10^{27}
North Korea	29 Sep 1973	89	593	5.0×10^{27}
Fiji–Tonga–Kermadec	26 May 1932	†	560	4.0×10^{27}
Okhotsk	25 May 1907	201	548	3.7×10^{27}
Solomon Islands	18 Aug 1968	46	545	9.4×10^{26}
Philippines	05 Mar 1984		644	9.3×10^{26}
Bonin–Marianas	30 May 1955	221	552	7.0×10^{26}

† = Non-CMT solutions. See Section 4.1.

We can also compare our results, derived from moments, to those found in p. 20 of Gutenberg and Richter (1954), who list as the four largest deep earthquakes the 1906 Japanese, 1932 Tonga, 1937 Tonga (this event could not be inverted) and 1950 Sea of Okhotsk earthquakes. We note that the use of magnitude obscured the true size of the 1921–1922 Peruvian earthquakes, and significantly overestimated the 1906 Japanese one.

In the shallower band, it is remarkable that three out of 10 earthquakes (but not the largest ones) are from the Bonin–Marianas subduction zone. As discussed later, this slab departs significantly from the other WBZs in the repartition of its seismicity with depth.

In the deeper band (500–690 km), we note that seven out of 13 earthquakes are from South America, but we stress that most of the major subduction zones are represented. Table 4 would argue that large events ($M_0 \geq 3\times10^{27}$ dyn-cm) can and do occur in most deep WBZs, the most notable exception being the Bonin–Marianas slab.

Another significant property in Table 3b is that all seven largest known deep events (possibly eight given the uncertainty on the moment of the 1932 shock) occur either in environments where the slab is known to be significantly bent or warped (e.g., in the Bolivian jog), or as isolated shocks with no known neighbors (e.g., Colombia, Spain). In the former case, this could be explained by an increase in ambient stresses due to the warping, as well as by a generally larger volume available for rupture (Kirby et al., 1996). The isolated gigantic events remain an unsolved challenge at this point.

4.2. Seismic energy release as a function of depth

We now turn our attention to the general distribution of seismicity with depth inside subduction zones. It has long been recognized that this distribution is irregular (p. 16 of Gutenberg and Richter, 1954; Abe and Kanamori, 1979; Vassiliou et al., 1984; Frohlich, 1989). Fig. 12 shows the distribution of the global number of earthquakes (above $m_b = 4.5$) with depth for the time windows corresponding to the Harvard data set (dashed bins) and the combined WWSSN and Harvard years (solid bins). The population of earthquakes decreases approximately exponentially with depth down to a minimum at about 320 km.

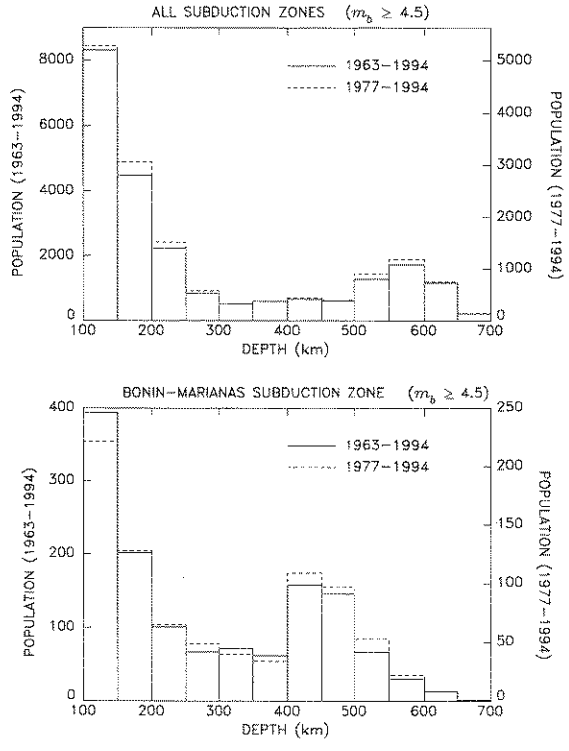

Fig. 12. Histogram of the number of earthquakes (with $m_b \geq 4.5$) as a function of depth, using the NEIC catalogue sampled in 50-km bins. Top: global population; Bottom: Bonin–Marianas subduction zone. Dashed lines and right scales are for the Harvard CMT era; Solid lines and left scales include the WWSSN years.

Below that, the distribution is slightly bimodal, with a peak at about 400 km, a much more pronounced one around 575 km, and a weak minimum about 500 km. All seismicity ceases at about 690 km; events occasionally quoted at greater depths have all been either successfully relocated at $h \leq 690$ km (Stark and Frohlich, 1985; Rees and Okal, 1987), or shown to have depth uncertainties making their hypocenters compatible with the above limit (Okal and Bina, 1998). Note that the two time windows give fundamentally the same distribution.

While most subduction zones generally follow the above pattern, there exist significant deviations away from it: in a few instances, total quiescence takes place over a particular depth range (400–550 km in South America; 300–500 km under Java; see Kirby et al., 1996 for discussion). Also the Marianas–Bonin slab is singular in that its maximum of activity takes place around 420 km, rather than 570 km, with comparatively little seismicity at the bottom of the slab (Fig. 12), the distribution being, again, the same for the two time windows.

There is, however, a significant variation in the general shape of the population if the seismicity is analyzed in any depth bin through the cumulative seismic moment released rather than the mere number of earthquakes. Fig. 13 uses 50-km depth bins for the years 1977–1994 covered by the Harvard CMT catalogue (note the logarithmic scale); we verified that the results of the binning procedure are robust with respect to a change of bin width. A comparison with Fig. 12 shows that the general bimodal character of the population below 300 km is maintained, but the first peak (at 420–450 km) is more prominent and the second one is sunk significantly to about 650 km.

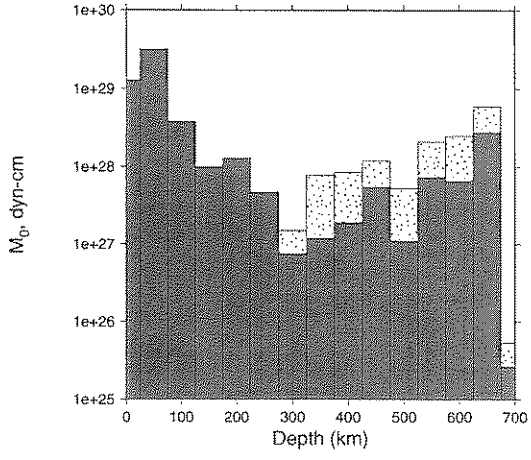

Fig. 13. Cumulative seismic release as a function of depth, sampled in 50-km bins. The filled bars refer to the Harvard CMT catalogue, while lighter bars include our WWSSN solutions.

The analysis of the variation of seismicity with depth is important, since it obviously illustrates changing conditions in the seismogenic material. For example, in the framework of the probable presence of a domain of metastability of mantle phases such as olivine in the interior of cold downgoing slabs, the existence of the two maxima in earthquake population has been interpreted as evidence for zones of increased stress in the metastable wedge. Denlinger and Kirby (1991) have argued that asymmetric rates of transformation below and above the wedge could create flexural stresses in the wedge, with its upper part in tension, and its lower part in compression. The flexural stresses would be significant at depths of 350–450 km where the differential bulk transformation is highest, which would explain one of the seismicity peaks (Kirby et al., 1996). The second peak could be due to internal stresses induced from volume reduction caused by phase transformation in material surrounding the wedge. The largest such stresses would be expected near the tip of the metastable wedge, which would cause a maximum of seismicity at about 600 km (Goto et al., 1987; Kirby et al., 1991). In another model, Bina (1996) has shown that a population curve such as the global one on Fig. 12 closely parallels the variation of down-dip stress in the slab as modeled by integrating buoyancy forces expressing differences in density between metastable phases, transformed phases and warmer ambient mantle.

Here, we study the input of the new enhanced data set to our understanding of the regime of moment release as a function of depth. While studies based on the Harvard CMT catalogue alone and on the combined Harvard and WWSSN data set show generally similar patterns, Fig. 13 does reveal several significant differences. Most importantly, the trough at 300–400 km is much less pronounced in the combined data set. This is due to the occurrence of three very large earthquakes, namely the 1962 Fiji ($h = 396$ km; $M_0 = 2.0 \times 10^{27}$ dyn-cm), the 1972

Table 5
Largest moments from various catalogues and in selected depth ranges

Depth range (km)	Harvard CMT (1977–1990)	Harvard CMT (1977–1994)	Harvard + WWSSN (1962–1994)	Harvard + WWSSN + historical (1907–1994)	Others
0–100	Indonesia 1977 (**36**)				Chile 1960 (**2000**)
100–275	Kuriles 1978 (**6.4**)				Argentina 1950 (**26**)
275–325	Kermadec 1981 (**0.08**)	Fiji 1991 (**0.31**)		New Zealand 1953 (**0.76**)	
325–375	South of Japan 1989 (**0.04**)	South of Japan 1993 (**0.25**)	Sulawezi (*82*) 1972 (**4.7**)		
375–425	So. of Japan 1984 (**0.61**)	Fiji 1992 (**0.78**)	Fiji (*2*) 1962 (**2.0**)		
425–475	Banda Sea 1982 (**1.8**)			Fiji (*225*) 1956 (**2.7**)	
475–525	Solomon Island 1980 (**0.15**)	Sea of Japan 1994 (**1.10**)	Bonin Island (*49*) 1968 (**1.14**)		
525–575	Fiji 1986 (**0.56**)	Fiji 1994 (**3.1**)	Peru–Bolivia (*7*) 1963 (**3.9**)		Fiji 1932 (≈ **4**)
575–625	Sakhalin 1990 (**0.82**)		North Korea (*89*) 1973 (**5.0**)		Indonesia 1996 (**7.9**)
625–675	Mindanao 1984 (**0.93**)	Bolivia 1994 (**26**)			
> 675	Tonga 1977 (**0.02**)				

All moments are given in **bold** in units of 10^{27} dyn-cm. A box is filled only if it results in a moment greater than the previous one to the left. Solutions obtained in the present study are indexed in *italics*.

Celebes Sea ($h = 332$ km; $M_0 = 4.7 \times 10^{27}$ dyn-cm), and the 1972 Solomon Islands ($h = 420$ km; $M_0 = 7.8 \times 10^{26}$ dyn-cm) events. Note, however, that since our study was limited a priori to $h \geq 300$ km, the 300-km bin could be undersampled during the WWSSN years.

On the other hand, the occurrence of the large very deep shocks of 1970 in Colombia ($h = 651$ km; $M_0 = 1.4 \times 10^{28}$ dyn-cm), 1973 in North Korea ($h = 593$ km; $M_0 = 5.0 \times 10^{27}$ dyn-cm) and 1963 in Peru–Bolivia ($h = 596$ km; $M_0 = 3.5 \times 10^{27}$ dyn-cm) maintain the pattern of energy release in the deepest parts of the slabs. The minimum around 500 km is confirmed as is the rapid decay at the very bottom of the slabs ($h \geq 670$ km). On the other hand, Fig. 12 indicates that the repartition of the number of events with depth was very stable during and after the WWSSN years.

Because the historical catalogue (pre-1962) does not feature completeness, it cannot be used for a study of cumulative energy release. An alternative approach consists of studying the largest known earthquake in selected depth bins (Table 5), as documented by the various available catalogues. These results are also presented on Fig. 14. Because this study is concerned only with deep earthquakes, we regroup all seismicity above 275 km in just two bins: shallow (0–70 km) and upper intermediate (70–275 km). Starting with the Harvard CMT data set as it existed when the present study was initiated in 1993 (it was then current to the end of 1990), we plot for each bin the largest known moment. We then improve on this catalogue by adding successively the 1991–1994 years of the Harvard data set, the WWSSN years and the historical data set. Finally, we include our knowledge of 'other' sources including the 1960 Chilean and 1950 Argentinian earthquakes, as documented by Kanamori and Cipar (1974) and Okal (1992), the 1932 Tonga earthquake as studied by Okal (1997) and the recent 1996 Indonesian earthquake. Note that we keep the 1970 Colombian earthquake at 651 km, in agreement with Gilbert and Dziewonski (1975). We also include in the historical data set the New Zealand earthquakes originally listed as deeper than 300 km, but which were dropped from our catalogue when their inverted depths turned out to be less than 300 km (Huang et al., 1997).

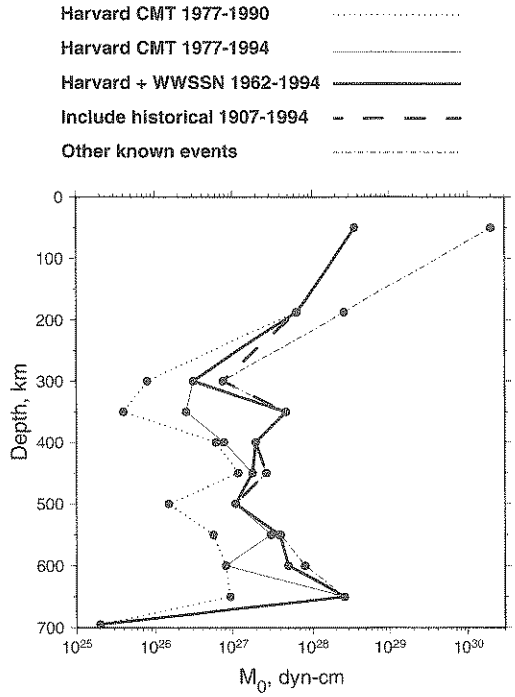

Fig. 14. Largest known seismic moment as a function of depth (using 50-km bins except for shallower layers). The various curves correspond to different datasets; see text for details.

It is immediately apparent that the WWSSN data set improves considerably upon the Harvard catalogue. It eliminates the apparent lows in maximum earthquake size at 350 and 600 km and suggests that earthquakes in the range of a few times 10^{27} dyn-cm can occur throughout the depth range at and below 350 km, with only a possible minimum around 500 km. Only time will tell if the latter is an artifact of undersampling.

5. A search for non-double-couple components of deep earthquakes

In this section, we use the enhanced data set obtained by combining the Harvard CMT catalogue with our new WWSSN and historical solutions, to reopen the question of the possible systematic deviation of deep earthquake sources from the simple model of a pure double-couple. We refer to Jost and Herrmann (1989) for a description of the decomposi-

tion of any second-order stress tensor into isotropic, double-couple, and compensated linear vector dipole (CLVD) components. Given a focal solution described by a moment tensor M_{ij} with eigenvalues σ_1, σ_2, and σ_3 ($\sigma_3 < \sigma_2 < \sigma_1$), we measure the non-double-couple component, or CLVD as

$$\varepsilon = \frac{-\sigma_2}{\max[|\sigma_1|,|\sigma_3|]} = \frac{\sigma_1 + \sigma_3}{\max[\sigma_1, -\sigma_3]} \quad (2)$$

Note that the standard CMT algorithm constrains the isotropic part of the moment tensor, M_{ii}, to zero, and hence, $\sigma_1 + \sigma_2 + \sigma_3 = 0$ in all our solutions. This reflects the fact that the combination M_{ii} is poorly resolved since its kernels are generally smaller than those of deviatoric components, especially for deep sources and at high frequencies (e.g., Okal and Geller, 1979).

If $\sigma_2 = 0$, the source is a pure double-couple with $\varepsilon = 0$. A 'pure CLVD' source corresponds to $\varepsilon = \pm 0.5$. Such a source can be visualized as the superposition of two double-couples for which the compression and null axes (or tension and null axes) have been permuted.

Previous work has revealed that earthquakes at all depths commonly feature observable CLVD components (Giardini, 1984; Frohlich, 1989), the average values for the entire Harvard catalogue being $\langle \varepsilon \rangle = -0.2\%$, $\langle |\varepsilon| \rangle = 12.4\%$. For deep earthquakes ($h = 300$ km), these values are practically identical ($\langle \varepsilon \rangle = -0.2\%$, $\langle |\varepsilon| \rangle = 11.6\%$). A favored explanation of the origin of CLVD components in deep shocks is that they reflect the superposition during the failure process of two or more subevents with different double-couple mechanisms (Frohlich, 1989; Kuge and Kawakatsu, 1992). Indeed, several detailed studies have shown evidence for multiple events with distinct mechanisms in the rupture process of intermediate and deep earthquakes (Strelitz, 1980; Choy and Boatwright, 1981; Lundgren et al., 1988), although for the more recent 1994 earthquakes in Fiji and Bolivia, Goes and Ritsema (1995) and Lundgren and Giardini (1995) identified only small deviations in geometry during the ruptures. Also, based on laboratory experiments on ice, Kirby et al. (1991) have suggested that non-double-couple source mechanisms may result from the presence of multiple transformational faults with different orientations. Other possible mechanisms at shallow depths, such as the opening of a tensile crack under fluid pressure (Julian and Sipkin, 1985) or slip along a curved fault surface (Frohlich, 1990; Ekström, 1994), are probably less relevant to the CLVD components of deep events.

The mineralogical structure in the cold interior of a slab is controlled by its temperature, itself governed by a combination of factors such as depth, lithospheric age at the time of subduction and speed of subduction. As a result, the metastable wedge is expected to shrink in width as the slab penetrates deeper. Indeed, Okal and Kirby (1995) have argued that different slab widths could account for a variation in the population characteristics of deep earthquakes in subduction zones with different thermal parameters. As the width of metastable material within the slab is expected to be no more than a few (perhaps at most 20) km, Houston (1993) has pointed out that the source of large deep earthquakes may not fit inside that restricted seismogenic zone, and proposed that faulting occur on multiple fault planes, a scenario generally upheld by the en échelon model of Chen (1995) for the rupture of the 1994 Bolivian earthquake. Houston's model would then suggest that the tight space available for rupture in a large deep earthquake would force it to rupture on a system of multiple faults, which would predict greater than average CLVD components for large deep earthquakes, especially near the tip of the wedge. On the other hand, Giardini (1984) observed that on average, the CLVD component decreased with increasing moment. The data sets used in both above studies were, however, of limited size.

According to the definition of ε, a negative value indicates that the largest principal stress represents compression, whereas a positive CLVD would represent tension. If, during a multiple rupture, the tectonically controlled principal stress remains coherent while the other nonzero principal stress fluctuates as a result of a change in geometry, the resulting CLVD should keep the signature of the former. Thus one would expect more events with negative CLVD values since the lithosphere acts as a stress guide with predominantly down-dip compression (e.g., Isacks and Molnar, 1971).

We examine here the CLVD components of large deep events using the combined Harvard and WWSSN CMT solutions (1962–1994). Fig. 15 shows

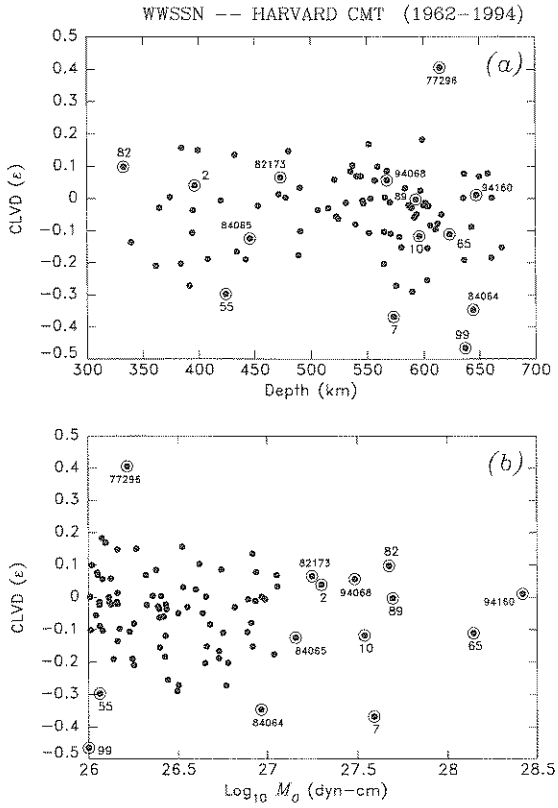

Fig. 15. CLVD component ε as defined by Eq. (2), plotted as a function of depth (Top) and main double-couple moment (Bottom) for all earthquakes in the combined Harvard and WWSSN dataset with $M_0 \geq 10^{26}$ dyn-cm. Events featuring either a large $|\varepsilon|$ or one of the 10 largest moments are outlined, and listed in Table 6.

the CLVD fraction as a function of depth and moment for deep events with $M_0 \geq 10^{26}$ dyn-cm. Individual earthquakes are shown by solid and open circles. The 10 largest events in the catalogue, and four events selected for their large CLVD components, are outlined, and identified either by their index in Huang et al. (1997) (WWSSN events), or their Julian date (Harvard CMT catalogue). All relevant source information is listed in Table 6.

Among the 10 largest deep earthquakes, only the great Peru–Bolivia shock of 15 August 1963 (Number 7) features a dominant, strongly negative, non-double-couple component, a property already evidenced in the study of Gilbert and Dziewonski (1975). This would suggest that the other large deep events, expected to be confined in a narrow seismogenic zone, may find alternative regimes of complex rupture not giving the appearance of a CLVD source. Typical examples would be the great 1994 earthquakes in Bolivia and Fiji which are posterior to the study of Houston (1993), but whose CLVD components are minimal (1% and 6%, respectively). For the former, one notes that the source orientation changes very little during rupture (Lundgren and Giardini, 1995; Goes and Ritsema, 1995) even though the position of the rupture in space may jump in an en échelon fashion (Chen, 1995). For the latter, Wiens et al. (1994) have proposed that its rupture may have penetrated outside the 'seismogenic' zone, as defined by background seismicity, without a significant change in fault geometry.

As for the events exhibiting the strongest CLVD component, they did occur towards the bottom of their respective subduction zones, all of which would have been expected to be particularly narrow given their unfavorable thermal parameters. They showed, however, both positive (77296) and negative (99, 84064) values of ε. Finally, note that the combined deep earthquake data set (1962–1994) has $\langle|\varepsilon|\rangle = 0.11$ which differs insignificantly from the average over the full range of depths in the Harvard data set ($\langle|\varepsilon|\rangle = 0.12$).

In an attempt to find any systematic correlation of ε with depth or moment, we regressed our data set against these parameters, and obtained the following least-squares slopes: -0.52×10^{-4} km^{-1} for ε as a function of depth (or -0.5% per 100 km); -0.25×10^{-5} km^{-1} for $|\varepsilon|$ as a function of depth (or 0.02% per 100 km); -0.016 for ε as a function of $\log_{10} M_0$ (or -4% for the entire range of Fig. 14); -0.008 for $|\varepsilon|$ as a function of $\log_{10} M_0$ (or -2% for the entire range of Fig. 15).

Regarding the historical (pre-1962) data set, the CLVD distribution is presented on Fig. 16. The average values of the CLVD parameter are $\langle\varepsilon\rangle = 0.05$; $\langle|\varepsilon|\rangle = 0.19$. These are larger than for the WWSSN data set, and could correspond to a degradation of the quality of the solutions. On the other hand, the largest absolute values ($\varepsilon = 0.38$ for the 1928 event South of Honshu or $\varepsilon = 0.43$ for the 1939 Sakhalin earthquake) are comparable to the largest values among the Harvard solutions ($\varepsilon = -0.35$ and $\varepsilon = 0.41$; see Table 6).

Table 6
The 10 largest deep earthquakes and deep events with large absolute CLVD components ($|\varepsilon| \geq 0.30$) for the years 1962–1994

Index	Date	Area (km)	Depth (dyn-cm)	Moment	ε
94160	09 Jun 1994	North Bolivia	647	2.6×10^{28}	0.01
65	31 Jul 1970	Colombia	623	1.4×10^{28}	−0.11
89	29 Sep 1973	North Korea	593	5.0×10^{27}	0.00
82	11 Jun 1972	Celebes Sea	322	4.7×10^{27}	0.10
7	15 Aug 1963	Peru–Bolivia	573	3.9×10^{27}	−0.37
10	09 Nov 1963	Peru–Bolivia	573	3.5×10^{27}	−0.12
94068	09 Mar 1994	Fiji Islands	568	3.1×10^{27}	0.06
2	21 May 1962	Fiji Islands	568	2.0×10^{27}	0.04
82173	22 Jun 1982	Banda Sea	473	1.8×10^{27}	0.07
84065	06 Mar 1984	South Honshu	446	1.4×10^{27}	−0.12
99	23 Jan 1976	Flores Sea	637	1.0×10^{26}	−0.47
77293	22 Oct 1977	Argentina	615	1.6×10^{26}	0.41
84064	05 Mar 1984	Mindanao	644	9.3×10^{26}	−0.35
55	31 Mar 1969	Japan Sea	424	1.2×10^{26}	−0.30

We have verified that all the above results are not significantly different when including the smaller earthquakes ($M_0 < 10^{26}$ dyn-cm), which would be expected to be unaffected by the constrained environment at the tip of the seismogenic zone in the slab. We conclude that our data set, which substantially enhances the Harvard CMT catalogue, does not suggest any particular trend in the values of ε for large earthquakes, either with depth or moment. Nor is there a trend towards exhibiting larger CLVD components, the latter being characterized by the absolute value $|\varepsilon|$.

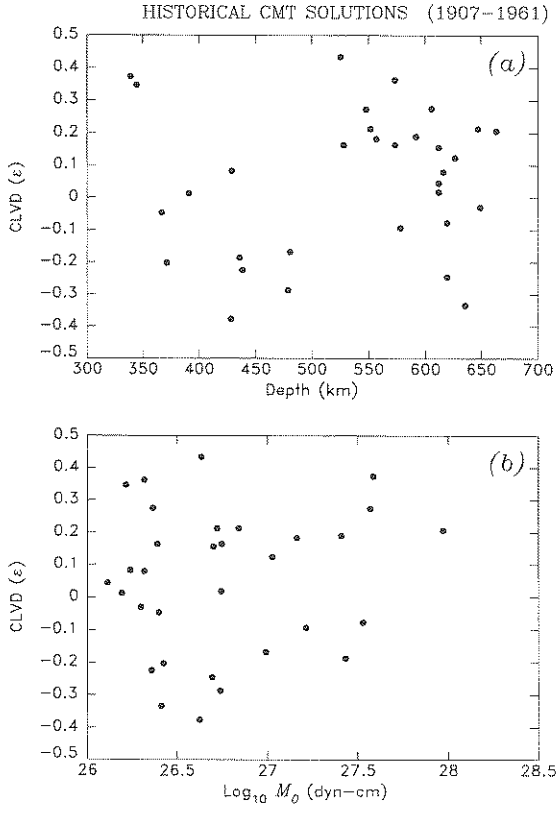

Fig. 16. Same as Fig. 15 for the historical CMT solutions.

Finally, an examination of the CLVD components of the Bonin–Marianas deep earthquakes would reveal a possible systematic increase of ε with depth (with a slope of 5% per 100 km) for events above 10^{26} dyn-cm, which however disappears if smaller earthquakes are included). No trend with size can be detected. In this respect, the anomalous character of the Bonin–Marianas zone does not extend to the generation of significant non-double-couple components.

6. Conclusions

(1) Our new data set of 139 CMT solutions significantly complements the existing Harvard data set. In several regions, it provides geographical continuity where the Harvard solutions were undersampling the true level of seismicity. For example, it reaffirms the existence of a continuous finger of

seismicity under Sakhalin, and it fills what were perceived as several seismicity gaps.

(2) Little if any evidence is found for the preferential location of large events at the lateral extremities of active WBZs, as was suggested from data sets using magnitude estimates for historical earthquakes. This is the case in particular under Java and at the Southern end of the South America WBZ, where comparable or larger events are found in the center of the relevant slabs. Rather, we find that the largest deep earthquakes have a tendency to occur either in areas of significant slab bending or warping, or as isolated events (such as the Colombian and Spanish deep shocks).

(3) In general, most previously published focal solutions based on WWSSN seismograms are found to agree well with our inverted focal mechanisms. Solutions for pre-WWSSN events, on the other hand, bear no significant correlation with our CMT-inverted mechanisms, and should probably be considered as unreliable.

(4) We shed new light on the repartition of seismic moment release with depth. The local maximum at 450 km may be less pronounced than apparent from the recent (Harvard) data set. The local minimum at 500 km seems confirmed, as is the significant maximum of seismic release at 650 km. Our data set indicates that large earthquakes ($M_0 \geq 10^{27}$ dyn-cm) can be expected at all depths, including around 300 and 500 km, and in most subduction zones.

(5) Predigital events confirm the most significant exception to the above patterns: the Bonin–Marianas subduction zone for which the maximum of seismic release takes place between 400 and 500 km. In addition, the maximum size of deep earthquakes is the smallest among all subduction zones. The origin of this behavior remains unclear.

(6) The enhanced data set does not reveal any resolvable trend regarding non-double-couple components of the moment tensor. While our new solutions confirm their ubiquitous occurrence, we could not find any systematic correlation with either depth, size of even age of the event. This suggests that the mechanism by which such components are developed must be more complex than predicted by simple models based on the expected geometry of the seismogenic zone.

Acknowledgements

The inversion of the predigital CMT solutions was carried out in collaboration with Harvard University, and we thank Göran Ekström and Misha Salganik for their valuable help over several years. We acknowledge many discussions with Steve Kirby, Craig Bina and Seth Stein. Robin Adams kindly attempted to relocate the 1907 Sea of Okhotsk earthquake. Many figures were drafted using the GMT software (Wessel and Smith, 1991). We are grateful to Cliff Frohlich for a careful review. This research was supported by the National Science Foundation under grant EAR-93-16396.

References

Abe, K., Kanamori, H., 1979. Temporal variation of the activity of intermediate- and deep-focus earthquakes. J. Geophys. Res. 84, 3589–3595.

American Association of Petroleum Geologists, 1987. Plate tectonic map of the circum-Pacific region, Tulsa.

Averyanova, V.N., 1973. Seismic Foci in the Far East. Israel Program for Scientific Translations, Jerusalem.

Barazangi, M., Dorman, J., 1969. World seismicity maps compiled from ESSA, Coast and Geodetic Survey, epicenter data, 1961–1967. Bull. Seismol. Soc. Am. 59, 369–380.

Berckhemer, H., Jacob, K.H, 1968. Investigation of the dynamical process in earthquake foci by analyzing the pulse shape of body waves. Institute of Meteorology and Geophysics, University of Frankfurt, Frankfurt am Main, 85 pp.

Bina, C.R., 1996. Phase-transition buoyancy contributions to stresses in subducting lithosphere. Geophys. Res. Lett. 23, 3563–3566.

Buland, R.P., Gilbert, F., 1976. Matched filtering for the seismic moment tensor. Geophys. Res. Lett. 3, 205–206.

Chandra, U., 1970. The Peru–Bolivia border earthquake of August 15, 1963. Bull. Seismol. Soc. Am. 60, 639–646.

Chase, C.G., 1971. Tectonic history of the Fiji plateau. Bull. Geol. Soc. Am. 82, 3087–3110.

Chen, W.-P., 1995. En échelon ruptures during the great Bolivian earthquake of 1994. Geophys. Res. Lett. 22, 2261–2264.

Choy, G.L., Boatwright, J., 1981. The rupture characteristics of two deep earthquakes inferred from broadband GDSN data. Bull. Seismol. Soc. Am. 71, 691–712.

Denham, D., 1977. Summary of earthquake focal mechanisms for the Western Pacific–Indonesian region, 1929–1973. Report SE-3, US Dept. of Commerce, Boulder, 110 pp.

Denlinger, R.P., Kirby, S.H., 1991. Stresses imposed by the basalt–eclogite transformation in descending lithosphere. Eos. Trans. Am. Geophys. Un. 72, 481–482, [abstract].

Dziewonski, A.M., Woodhouse, J.H., 1983. An experiment in

systematic study of global seismicity: Centroid moment tensor solutions for 201 moderate and large earthquakes of 1981. J. Geophys. Res. 88, 3247–3271.

Ekström, G., 1994. Anomalous earthquakes on volcano ring–fault structures. Earth Planet. Sci. Lett. 128, 707–712.

Ekström, G., Dziewonski, A.M., Stein, J.M., 1986. Single-station CMT: Application to the Michoacan, Mexico earthquake of September 19, 1985. Geophys. Res. Lett. 13, 173–176.

Fitch, T.J., 1972. Plate convergence, transcurrent faults, and internal deformation adjacent to Southeast Asia and the Western Pacific. J. Geophys. Res. 77, 4432–4460.

Fitch, T.J., Molnar, P., 1970. Focal mechanisms along inclined zones in the Indonesian–Philippine region. J. Geophys. Res. 75, 1431–1444.

Frohlich, C., 1989. The nature of deep earthquakes. Annu. Rev. Earth Planet. Sci. 17, 227–254.

Frohlich, C., 1990. Note concerning nondouble-couple source components from slip along surfaces of revolution. J. Geophys. Res. 95, 6861–6866.

Fukao, Y., Kikuchi, M., 1987. Source retrieval for mantle earthquakes by iterative deconvolution of long-period P waves. Tectonophysics 144, 249–269.

Furumoto, M., Fukao, Y., 1976. Seismic moments of great deep shocks. Phys. Earth Planet. Interiors 11, 352–357.

Geller, R.J., 1976. Scaling relations for earthquake source parameters and magnitudes. Bull. Seismol. Soc. Am. 66, 1501–1523.

Giardini, D., 1984. Systematic analysis of deep seismicity: 200 centroid-moment tensor solutions to earthquakes between 1977 and 1980. Geophys. J. R. Astron. Soc. 77, 883–911.

Gilbert, F., Dziewonski, A.M., 1975. An application of normal mode theory to the retrieval of structural parameters and source mechanisms from seismic spectra. Philos. Trans. R. Soc. London, Ser. A 278, 187–269.

Goes, S., Ritsema, J., 1995. A broadband P wave analysis of the large deep Fiji Island and Bolivia earthquakes of 1994. Geophys. Res. Lett. 22, 2249–2252.

Goto, K., Suzuki, A., Hamaguchi, H., 1987. Stress distribution due to olivine–spinel transition in descending plate and deep focus earthquakes. J. Geophys. Res. 92, 13811–13820.

Gutenberg, B., Richter, C.F., 1954. Seismicity of the Earth and Associated Phenomena, 2nd edn. Princeton Univ. Press, 310 pp.

Houston, H., 1993. The non-double-couple component of deep earthquakes and the width of the seismogenic zone. Geophys. Res. Lett. 20, 1787–1790.

Huang, W.-C., 1996. Centroid-moment tensor inversions of analog seismograms from deep earthquakes (1907–1976). PhD dissertation, Northwestern University, Evanston, 193 pp.

Huang, W.-C., Ekström, G., Okal, E.A., Salganik, M.P., 1994. Application of the CMT algorithm to analog recordings of deep earthquakes. Phys. Earth Planet. Interiors 83, 283–297.

Huang, W.-C., Okal, E.A., Ekström, G., Salganik, M.P., 1997. Centroid-moment-tensor solutions for deep earthquakes predating the digital era: The WWSSN data set (1962–1976). Phys. Earth Planet. Interiors 99, 121–129.

Huang, W.-C., Okal, E.A., Ekström, G., Salganik, M.P., 1998. Centroid moment tensor solutions for deep earthquakes predating the digital era: The historical data set (1907–1961). Phys. Earth Planet. Interiors (this issue).

Ichikawa, M., 1961. On the mechanism of the earthquakes in and near Japan during the period from 1950 to 1957. Geophys. Mag. 30, 355–404.

Isacks, B.L., Molnar, P., 1971. Distribution of stresses in the descending lithosphere from a global survey of focal-mechanism solutions of mantle earthquakes. Rev. Geophys. Space Phys. 9, 103–174.

Isacks, B.L., Sykes, L.R., Oliver, J., 1969. Focal mechanisms of deep and shallow earthquakes in the Tonga–Kermadec region and the tectonics of island arcs. Bull. Geol. Soc. Am. 80, 1443–1470.

Jost, M.L., Herrmann, R.B., 1989. A student's guide and review of moment tensors. Seismol. Res. Lett. 60, 37–57.

Julian, B.R., Sipkin, S.A., 1985. Earthquake process in the Long Valley Caldera area, CA. J. Geophys. Res. 90, 11155–11169.

Kagan, Y.Y., 1991. 3-D rotation of double-couple earthquake sources. Geophys. J. Int. 106, 709–716.

Kanamori, H., Cipar, J.J., 1974. Focal process of the great Chilean earthquake May 22, 1960. Phys. Earth Planet. Interiors 9, 128–136.

Kirby, S.H., Okal, E.A., 1996. Geodynamic implications of deep earthquakes in slabs stagnated in the transition zone: Deep seismicity beneath the Fiji Basin, SW Pacific. Eos. Trans. Am. Geophys. Un. 77 (46), F498, [abstract].

Kirby, S.H., Durham, W.B., Stern, L.A., 1991. Mantle phase changes and deep-earthquake faulting in subducting lithosphere. Science 252, 216–225.

Kirby, S.H., Okal, E.A., Engdahl, E.R., 1995. The 09 June 1994 great Bolivian deep earthquake: An exceptional deep earthquake in an extraordinary subduction zone. Geophys. Res. Lett. 22, 2233–2236.

Kirby, S.H., Stein, S., Okal, E.A., Rubie, D., 1996. Deep earthquakes and metastable mantle phase transformations in subducting oceanic lithosphere. Rev. Geophys. Space Phys. 34, 261–306.

Koyama, J., 1976. Source process of Vladivostok deep-focus earthquake of September 10, 1973. Sci. Rep. Tohoku Univ., Ser. 5. Geophys. 2, 83–101.

Kuge, K., Kawakatsu, H., 1992. Deep and intermediate-depth non-double couple earthquakes: Interpretation of moment tensor inversion using various passbands of very broadband seismic data. Geophys. J. Int. 111, 589–606.

Lundgren, P., Giardini, D., 1994. Isolated deep earthquakes and the fate of subduction in the mantle. J. Geophys. Res. 99, 15833–15842.

Lundgren, P., Giardini, D., 1995. The June 9 Bolivia and March 9 Fiji deep earthquakes of 1994: I. Source processes. Geophys. Res. Lett. 22, 2241–2244.

Lundgren, P.R., Okal, E.A., Stein, S., 1988. Body wave deconvolution for variable source parameters, application to the December 6, 1978 Kuriles earthquake. Geophys. J. 94, 171–180.

Mikumo, T., 1971. Source process of deep and intermediate earthquakes as inferred from long-period P and S waveforms: 2. Deep-focus and intermediate-deep earthquakes around Japan. J. Phys. Earth 19, 303–320.

Mikumo, T., 1972. Focal process of deep and intermediate earthquakes around Japan as inferred from long-period P and S waveforms. Phys. Earth Planet. Interiors 6, 293–299.

Oike, K., 1969. The deep earthquake of June 22, 1966 in Banda Sea: A multiple shock. Bull. Dis. Prev. Res. Inst., Kyoto Univ. Part 2 158, 55–65.

Oike, K., 1971. On the nature of the occurrence of intermediate and deep earthquakes. Bull. Dis. Prev. Res. Inst., Kyoto Univ. 20, 145–182.

Okal, E.A., 1992. Use of the mantle magnitude M_m for the reassessment of the seismic moment of historical earthquakes: II. Intermediate and deep events. Pure Appl. Geophys. 139, 59–85.

Okal, E.A., 1997. A reassessment of the deep Fiji earthquake of 26 May 1932. Tectonophysics 275, 313–330.

Okal, E.A., Bina, C.R., 1994. The deep earthquakes of 1921–1922 in Northern Peru. Phys. Earth Planet. Interiors 87, 33–54.

Okal, E.A., Bina, C.R., 1998. On the cessation of seismicity at the base of the transition zone. J. Seismol. (in press).

Okal, E.A., Geller, R.J., 1979. On the observability of isotropic seismic sources: The July 31, 1970 Colombian earthquake. Phys. Earth Planet. Interiors 18, 176–196.

Okal, E.A., Kirby, S.H., 1993. Quantitative reassessment of the intermediate and deep seismicity of the Indonesian arc: Preliminary results. Seismol. Res. Lett. 64, 14, [abstract].

Okal, E.A., Kirby, S.H., 1995. Frequency–moment distribution of deep earthquakes: Implications for the seismogenic zone at the bottom of slabs. Phys. Earth Planet. Interiors 92, 169–187.

Okal, E.A., Engdahl, E.R., Kirby, S.H., Huang, W.-C., 1995. Earthquake relocations in the Kuril slab: Was the 1990 Sakhalin event not isolated after all?. Eos. Trans. Am. Geophys. Un. 76 (17), S199, [abstract].

Rees, B.A., Okal, E.A., 1987. The depth of the deepest historical earthquakes. Pure Appl. Geophys. 125, 699–715.

Richter, F.M., 1979. Focal mechanisms and seismic energy release of deep and intermediate earthquakes in the Tonga–Kermadec region and their bearing on the depth extent of mantle flow. J. Geophys. Res. 84, 6783–6795.

Ripper, I.D., 1974. Some earthquake focal mechanisms in the New Guinea–Solomon Islands region, 1963–1968. Bur. Miner. Resour. Aust. Rep. (Canberra) 178.

Ritsema, A., 1965. The mechanism of some deep and intermediate earthquakes in the region of Japan. Bull. Earthquake Res. Inst. Tokyo Univ. 43, 39–52.

Sasatani, T., 1980. Source parameters and rupture mechanism of deep-focus earthquakes. J. Fac. Sci. Hokkaido Univ., Ser. 7. Geophys. 6, 301–384.

Stark, P.B., Frohlich, C.H., 1985. The depths of the deepest deep earthquakes. J. Geophys. Res. 90, 1859–1859.

Stauder, W., 1973. Mechanism and spatial distribution of Chilean earthquakes with relation to subduction of the oceanic plate. J. Geophys. Res. 78, 5033–5061.

Stauder, W., Mualchin, L., 1976. Fault motion in the larger earthquakes of the Kuril–Kamchatka arc and of the Kuril–Hokkaido corner. J. Geophys. Res. 81, 297–308.

Strelitz, R.A., 1980. The fate of downgoing slab: A study of the moment tensors from body waves of complex deep-focus earthquakes. Phys. Earth Planet. Interiors 21, 83–96.

Sykes, L.R., 1964. Deep-focus earthquakes in the New Hebrides region. J. Geophys. Res. 69, 5353–5355.

Teng, T.-L., Ben-Menahem, A., 1965. Mechanism of deep earthquakes from spectrum of isolated body wave signals. J. Geophys. Res. 70, 5157–5170.

Vassiliou, M.S., 1984. The state of stress in subducting slabs as revealed by earthquakes analyzed by moment tensor inversion. Earth Planet. Sci. Lett. 69, 195–202.

Vassiliou, M.S., Hager, B.H., Raefsky, A., 1984. The distribution of earthquakes with depth and stress in subducting slabs. J. Geodyn. 1, 11–28.

Wessel, P., Smith, W.H.F., 1991. Free software helps map and display data. Eos. Trans. Am. Un. 72, 441 and 445–446.

Wickens, A.J., Hodgson, J.H., 1967. Computer reevaluation of earthquake mechanism solutions, 1922–1962. Publ. Domin. Obs. 33 (I) 560 pp.

Wiens, D.A., McGuire, J.J., Shore, P.J., Bevis, M.G., Draunidalo, K., Prasad, G., Helu, S., 1994. A deep earthquake aftershock sequence and implications for the rupture mechanism of deep earthquakes. Nature 372, 540–543.

Wyss, M., 1970. Stress estimates for South American shallow and deep earthquakes. J. Geophys. Res. 78, 1529–1544.

Wyss, M., Molnar, P., 1972. Source parameters of intermediate and deep focus earthquakes in the Tonga arc. Phys. Earth Planet. Interiors 6, 279–292.